PSI Center for Photon Science

EPFL

Manuel Guizar-Sicairos :: Head of the Computational X-ray Imaging group :: Paul Scherrer Institute
Associate Professor :: École Polytechnique Fédérale de Lausanne

Chapter 5 – Phase retrieval and ptychography

PHYS-715 Physical Optics and Advanced Imaging

CXI

Outline

- X-ray imaging
- The phase problem (CDI)
- Ptychography
- Ultrafast X-ray imaging with free-electron lasers

X-ray imaging

Motivation and basics
Full-field vs. scanning

Why X-ray imaging? High penetration depth

X-rays offer the opportunity to look through otherwise opaque objects without disturbing them (too much)

Hand mit Ringen first "medical" X-ray 1895 Anna Bertha Ludwig's hand

Wilhelm Röntgen 1901 First Physics Nobel

X-ray tomography

Why X-ray imaging? Element specificity

X-ray photons can remove electrons from inner atom orbitals

The resulting fluorescence upon relaxation leaves an element specific signature

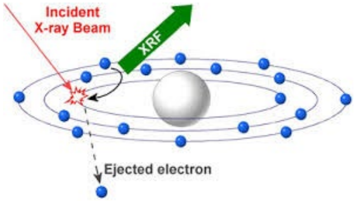

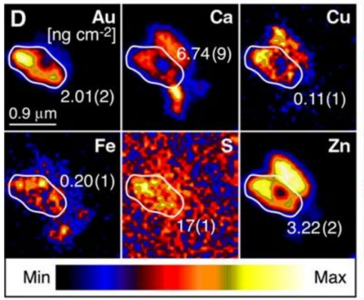

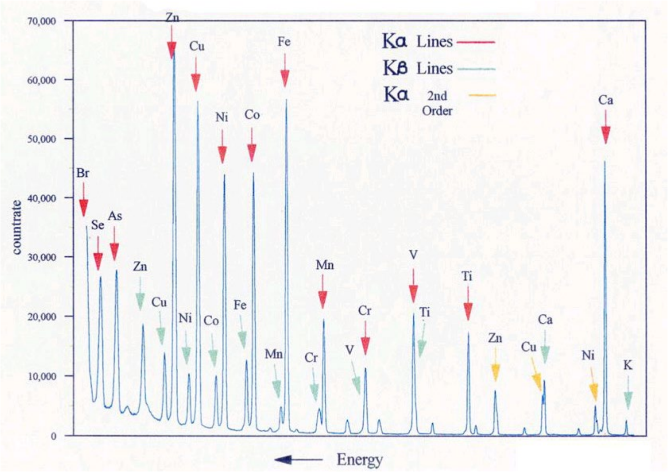

en.wikipedia.org

Why X-ray imaging? High resolution

Abbe theory of image formation:
Resolution depends on **wavelength** and **numerical aperture**. There is an upper limit for a given wavelength.

High-resolution = High diffraction angles

Rayleigh resolution

$$\Delta x = \frac{0.61\lambda}{n \sin\alpha}$$

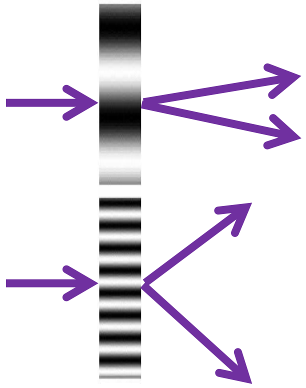

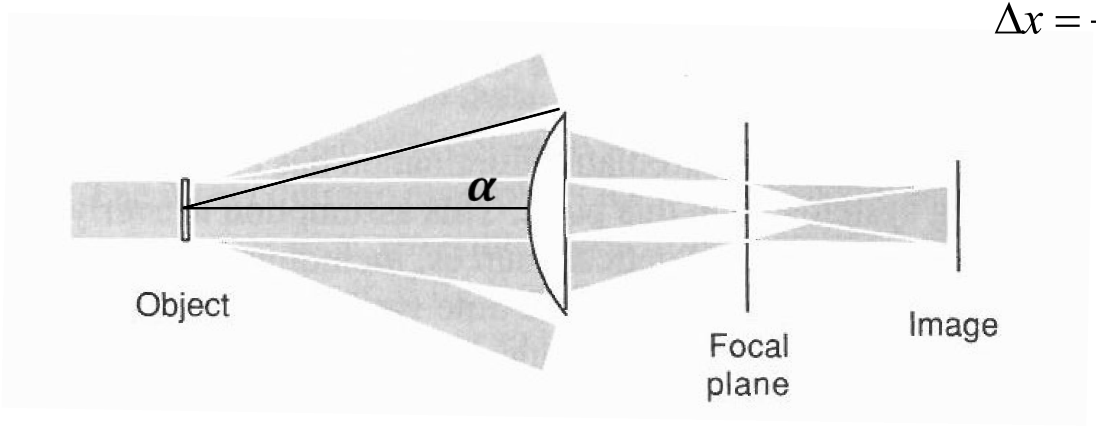

J. W. Goodman, Introduction to Fourier Optics, fourth edition. McMillan learning (2017)

Electromagnetic waves – Resolution

Image resolution depends on the numerical aperture of the lens, but there is a limit given by the wavelength.

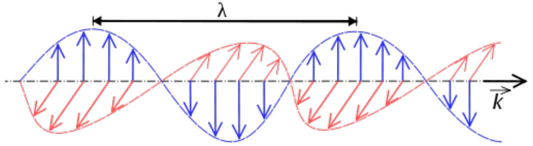

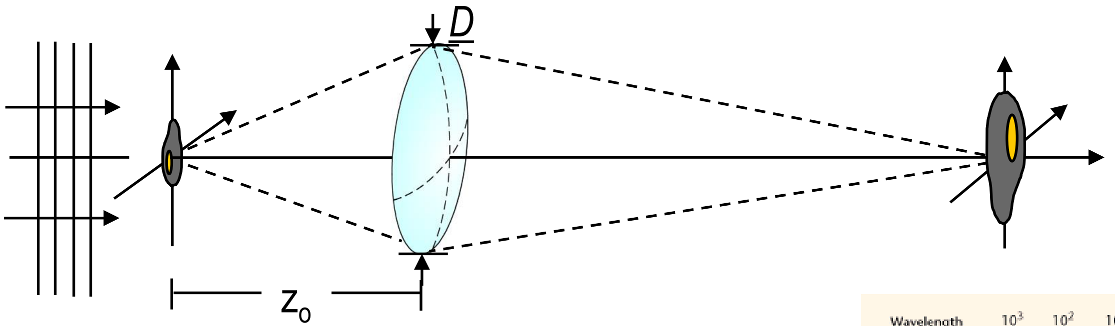

X-ray wavelengths then have great potential for high-resolution

$$\Delta x \approx 0.61\frac{\lambda}{NA} \approx 1.22\lambda(f\#) \approx 1.22\lambda\frac{z_o}{D}$$

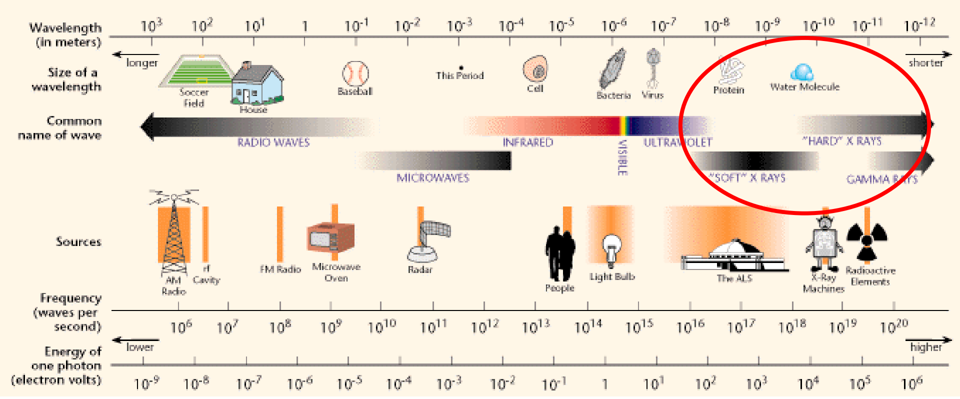

Full field imaging

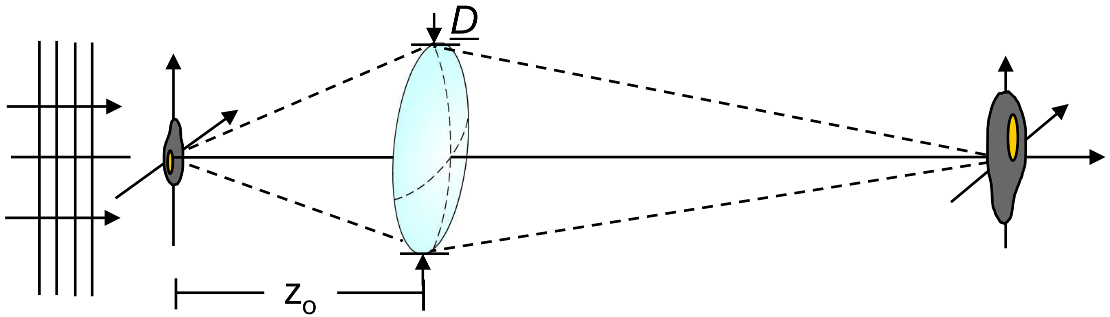

X-ray small wavelengths (0.01 – 10 nm) can potentially deliver high resolution

$$\Delta x \approx 0.61 \frac{\lambda}{NA}$$

Scanning

Fluorescence spectrum, photoelectrons

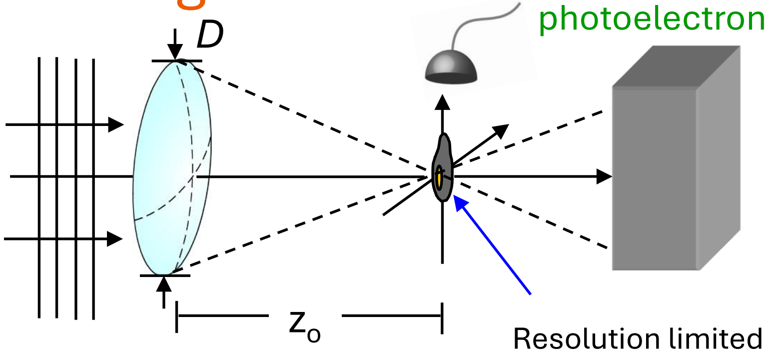

Resolution limited to size of the beam

measuring absorption
measuring reflection

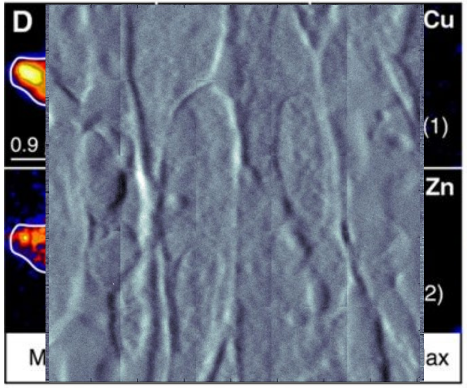

Andreas Menzel, Roger Wepf, *et al.*

Full field imaging

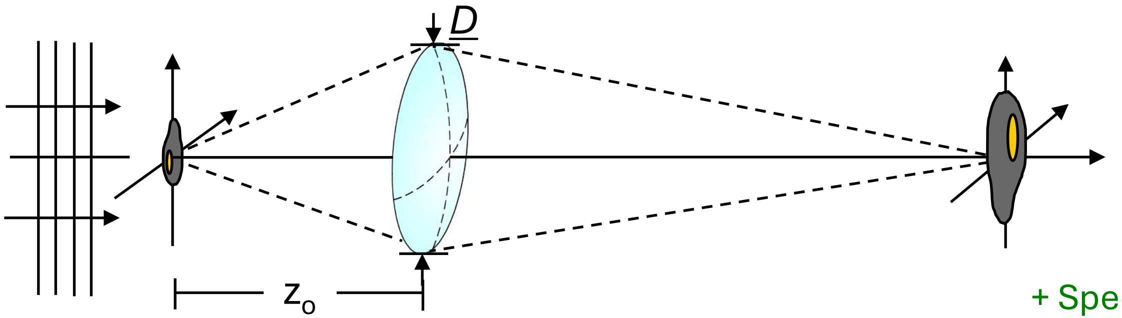

X-ray small wavelengths (0.01 – 10 nm) can potentially deliver high resolution

$$\Delta x \approx 0.61 \frac{\lambda}{NA}$$

+ Speed: Whole image measured at once
- Photon efficiency
- Background from other diffraction orders

Scanning

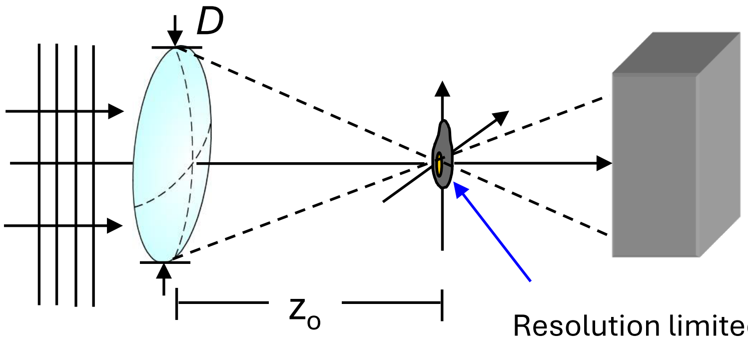

Resolution limited to size of the beam

+ Photon efficiency
+ Simultaneous imaging channels
- Speed: Point by point imaging
- More sensitive to drifts

Andreas Menzel, Roger Wepf, *et al.*

Outline

X-ray imaging

- The phase problem (CDI)

Ptychography

Ultrafast X-ray imaging with free-electron lasers

The phase problem (CDI)

Computational imaging - lensless
3D nanoscale imaging with CDI

Imaging as an inverse problem

Physical model of interaction between incoming wave and object

Diversity - Can be used to encode more information, e.g. rotation, scanning, energy

r (dimensionality) can be 2D, 3D, time, spectra

O (contrast) matter-wave interaction can be a scalar, vector, tensor
Captures local anisotropy

M (modulation and measurement) images, diffraction, fluorescence, photo-electrons

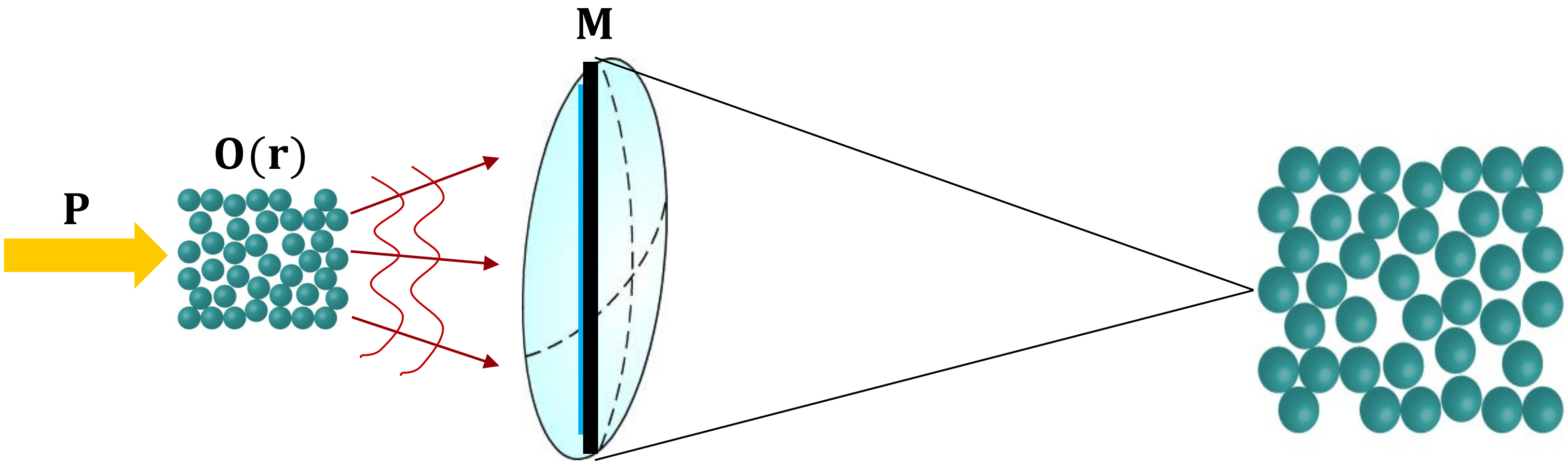

Imaging as an inverse problem

Physical model of interaction between incoming wave and object

Diversity - Can be used to encode more information, e.g. rotation, scanning, energy

r (dimensionality) can be 2D, 3D, time, spectra

O (contrast) matter-wave interaction can be a scalar, vector, tensor
Captures local anisotropy

M (modulation and measurement) images, diffraction, fluorescence, photo-electrons

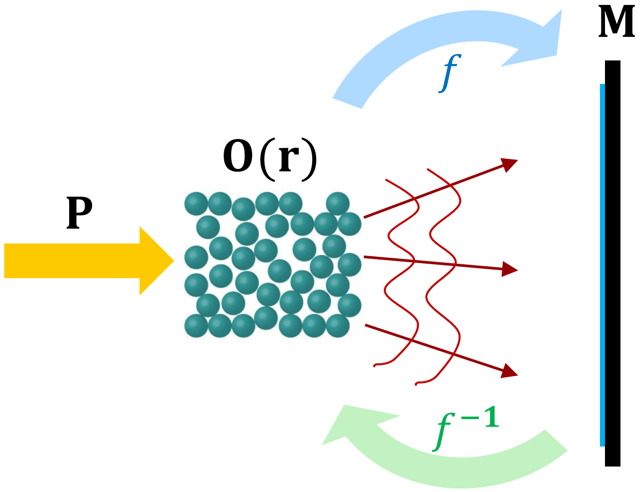

$$\mathbf{M} = f\,\{\mathbf{P}\cdot\mathbf{O}(\mathbf{r})\}$$

$$\mathbf{O}(\mathbf{r}) = f^{-1}\{\mathbf{M},\mathbf{P}\}$$

Diversity – measure in a way that makes the problem <u>invertible and stable</u> (small noise leads to small errors)

Find a reliable inversion strategy f^{-1}

X-ray coherent lensless imaging

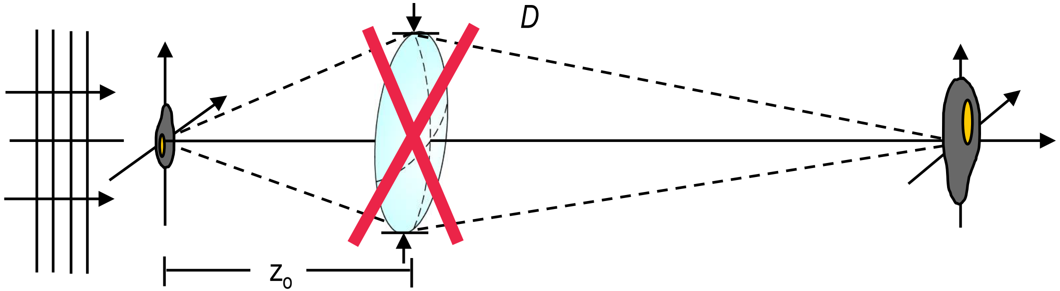

$$\Delta x \approx \frac{\lambda}{2NA} \approx \lambda(f\#) \approx \lambda\frac{z_o}{D}$$

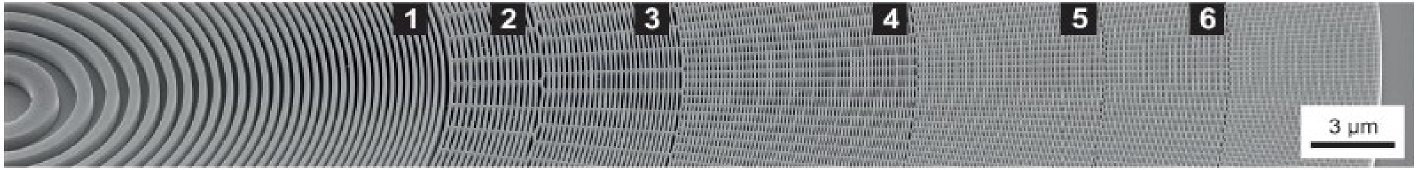

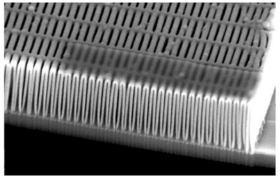

Line doubled, ZW 20 nm, H 550 nm
https://www.psi.ch/en/lxn/fresnel-zone-plate-for-x-ray-microscopy

Imaging resolution limited by lens manufacturing

An alternative is coherent lensless imaging

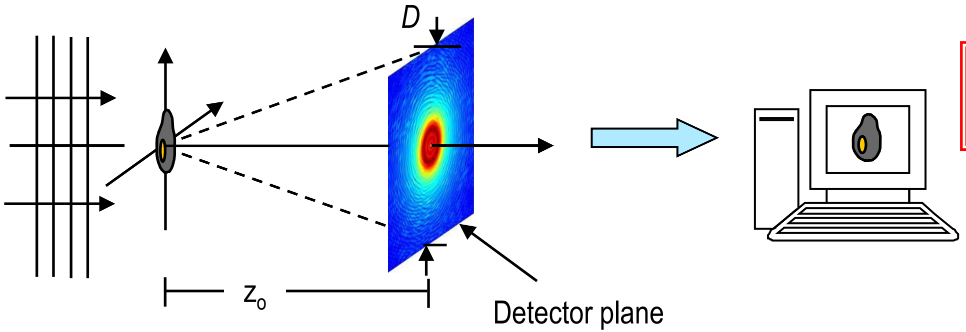

Complex-valued reconstruction

$$\Delta x \approx \lambda\frac{z_o}{D}$$

Synchrotron X-ray sources

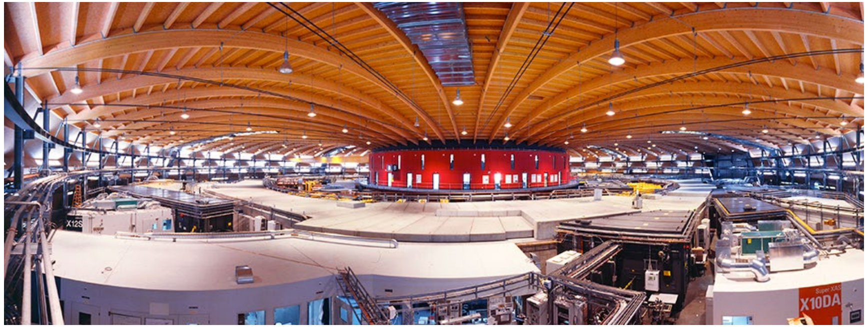

Swiss Light Source (SLS)

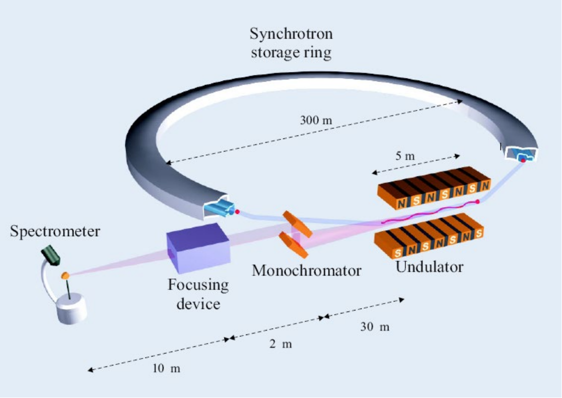

Figure from J. Als-Nielsen and D. McMorrow "Elements of modern X-ray physics"
www.psi.ch/en/sls

Synchrotrons have many beamlines with different experiments running simultaneously
Brightness ~ 1e6-1e9 higher than lab sources
Image: beamlines of Soleil (Wikipedia)

>75 years of synchrotrons

Scientists around the vacuum chamber of a 1947 General Electric synchrotron (photo courtesy of NSLS, Brookhaven).

Sirius - Brazilian synchrotron

https://www.esrf.fr/about/synchrotron-science/history-synchrotron
Sirius Aerial View - Credits: CNPEM 2020 Feb.

The 2D Fourier transform

The 2D FT is very important concept in optics, imaging, and tomography. It is a straightforward generalization of the 1D FT.

$f(x)$ → 1D FT → $F(u) = \int f(x) e^{-i2\pi(xu)} dx$

$f(x,y)$ → 2D FT → $F(u,v) = \iint f(x,y) e^{-i2\pi(xu+yv)} dxdy$

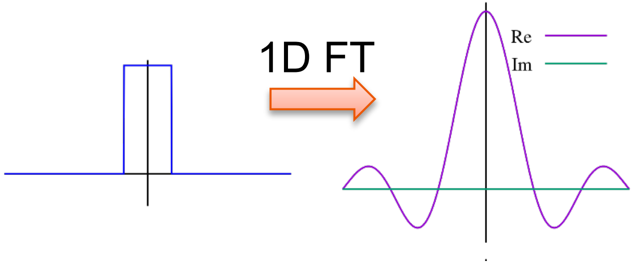

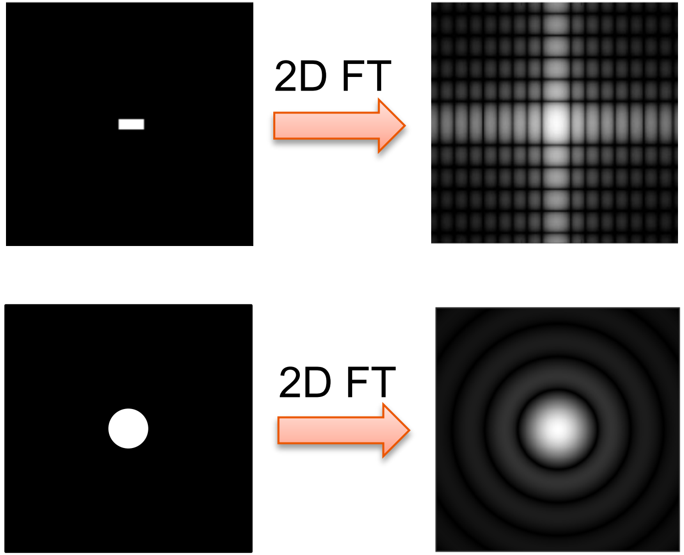

Images from https://en.wikipedia.org/ and https://www.chegg.com

Far-field (Fraunhofer) propagation

Optical propagation (far field) is reduced to a 2D FT

High resolution details propagate at higher angles

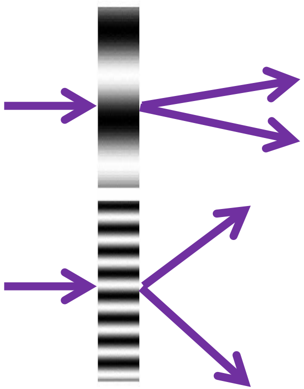

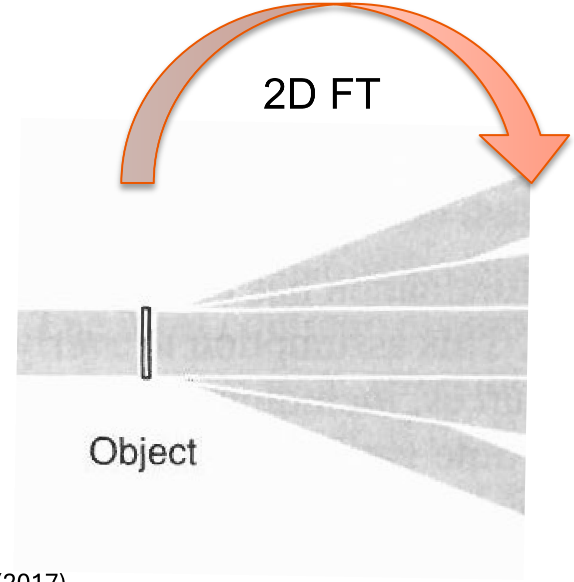

J. W. Goodman, Introduction to Fourier Optics, fourth edition. McMillan learning (2017)

The phase problem

Original object

Fourier transform

Propagation to the detector

Intensity

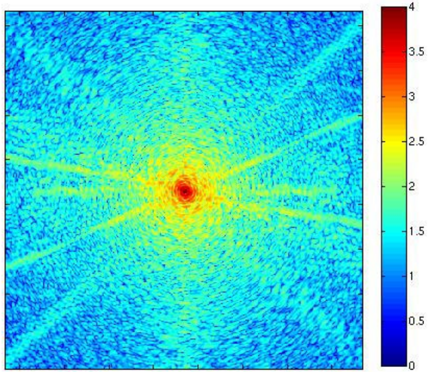

Object autocorrelation

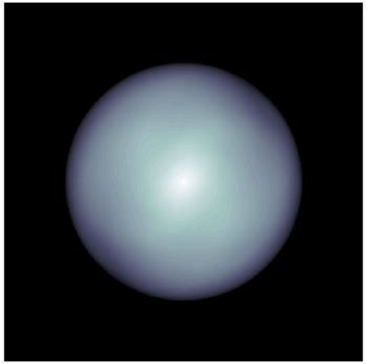

Numerical inverse Fourier transform

Phase is lost

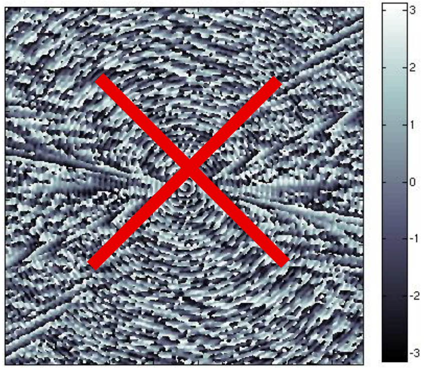

Phase retrieval with a support constraint (CDI)

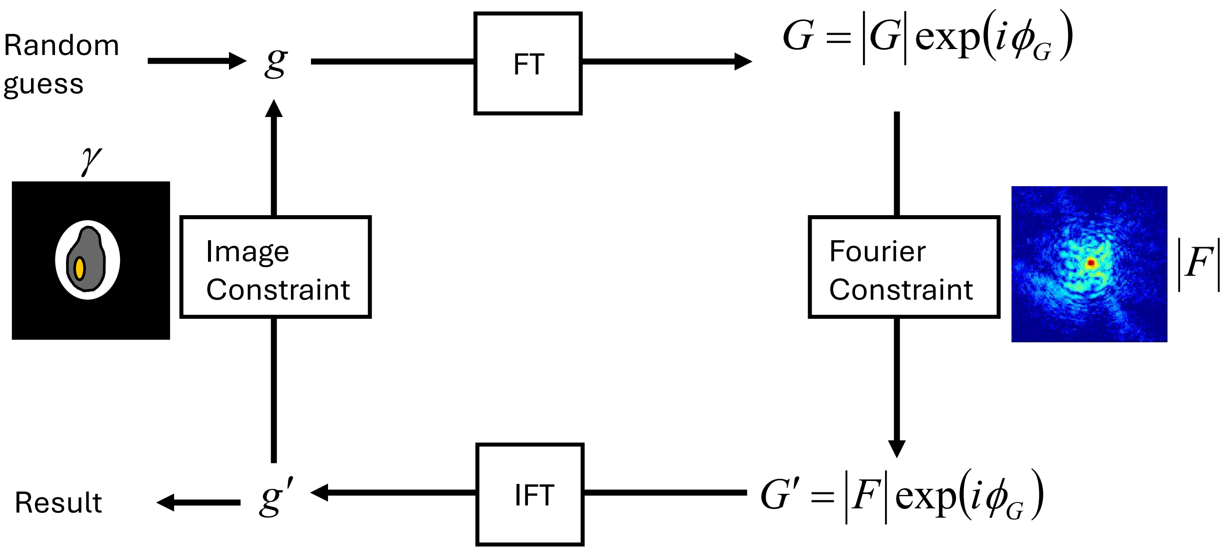

Robust algorithms have been developed, e.g. hybrid input-output and difference-map

Using the measured ***far-field intensity*** and the ***object support***

Note that additional constraints can be used

J. R. Fienup, "Phase retrieval algorithms: a comparison," Appl. Opt. 21, 2758-2769 (1982)

Hybrid Input-Output (HIO) Algorithm

Error reduction (Gerchberg–Saxton)

$$g_{k+1} = \begin{cases} g'_k & x \in \gamma \\ 0 & x \notin \gamma \end{cases}$$

HIO

$$g_{k+1} = \begin{cases} g'_k & x \in \gamma \\ g_k - \beta g'_k & x \notin \gamma \end{cases}$$

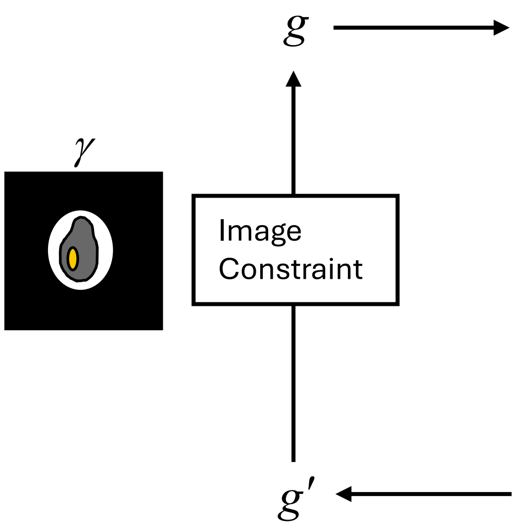

Instead of requiring the image to be zero outside the support, HIO uses the error as feedback.

Inspired in closed loop control theory.

Superior performance over the Error reduction (less prone to stagnation)

J. R. Fienup, “Phase retrieval algorithms: a comparison,” Appl. Opt. 21, 2758-2769 (1982)

Iterative projection – Gerchberg Saxton

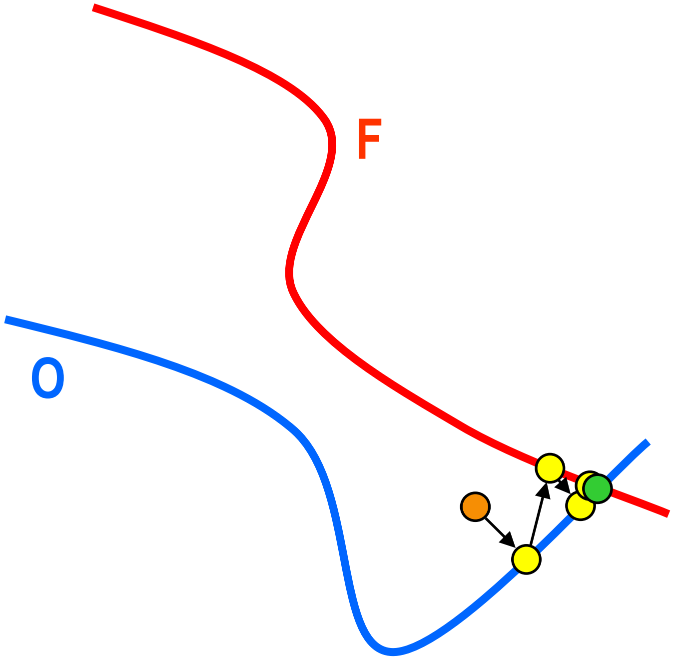

Project iteratively between object and Fourier constraints

Iterative projection – Gerchberg Saxton

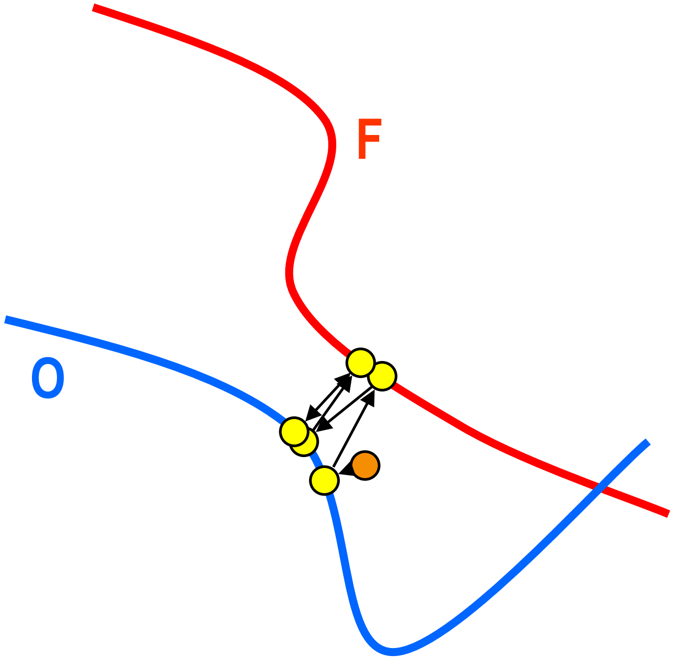

Project iteratively between object and Fourier constraints

Difference map – HIO

PSI
EPFL

$$\Psi_{n+1} = \Psi_n + \Pi_F[2\Pi_O(\Psi_n) - \Psi_n] - \Pi_O(\Psi_n)$$

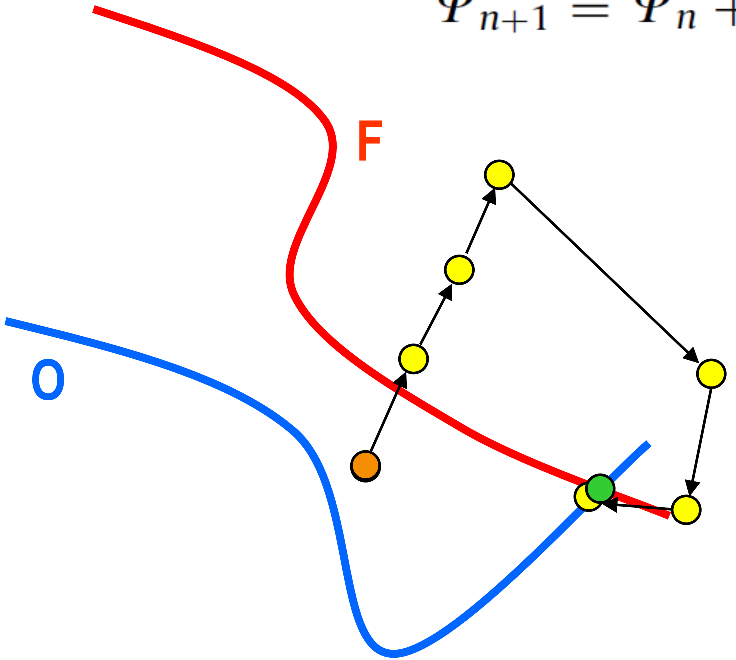

Use projections to find intersection between sets of constraints

Explore solution space and escapes local minima

Phase retrieval with a support constraint (CDI)

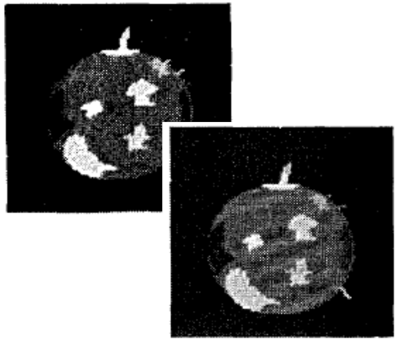

J. R. Fienup, Opt. Lett. **3**, 27 (1978)

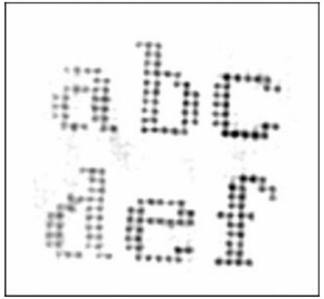

J. Miao et al., Nature **400**, 342 (1999)

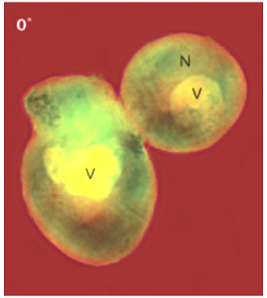

Specifically labeled freeze-dried yeast cell

J. Nelson *et al*., PNAS **107**, 7235 (2010)

Fourier projection-slice theorem

The Fourier transform of a parallel projection of an object *f(x,y)* obtained at an angle θ equals a line of the 2D Fourier transform of *f(x,y)* taken at the same angle.

$f(x, y)$

$$F(u, v) = \iint f(x, y) e^{-i2\pi(xu+yv)} dxdy$$

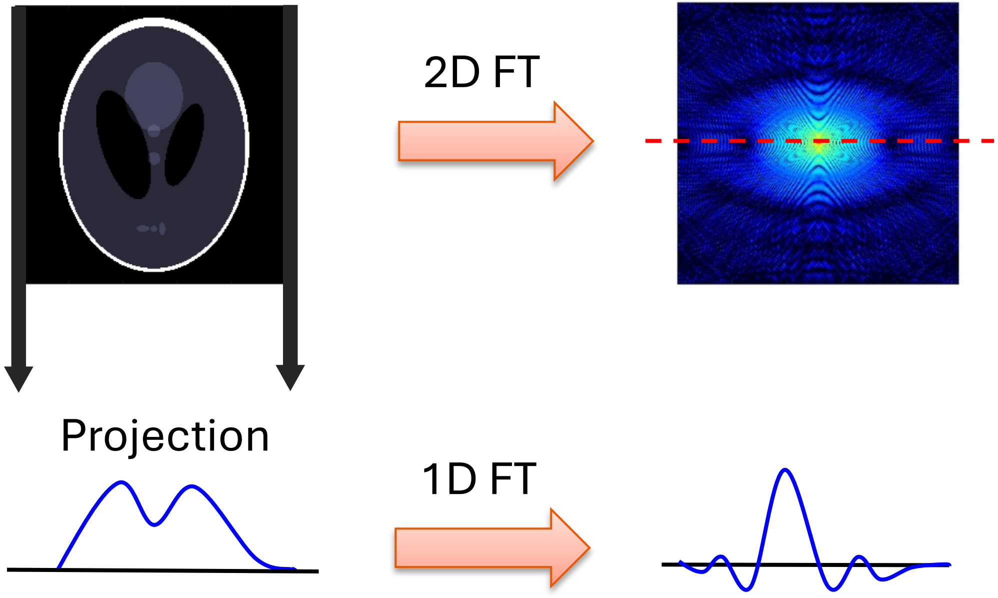

$$p(x) = \int f(x, y) dy$$

$$\iint f(x, y) e^{-i2\pi(xu)} dxdy \quad = F(u, 0)$$

3D measurement & reconstruction by phase retrieval

Attempt to reconstruct the scattering potential of the object *o*(*x*,*y*,*z*) by rotating the sample

$$o(x,y,z) \approx \frac{2\pi}{\lambda^2}\Delta n(x,y,z)$$

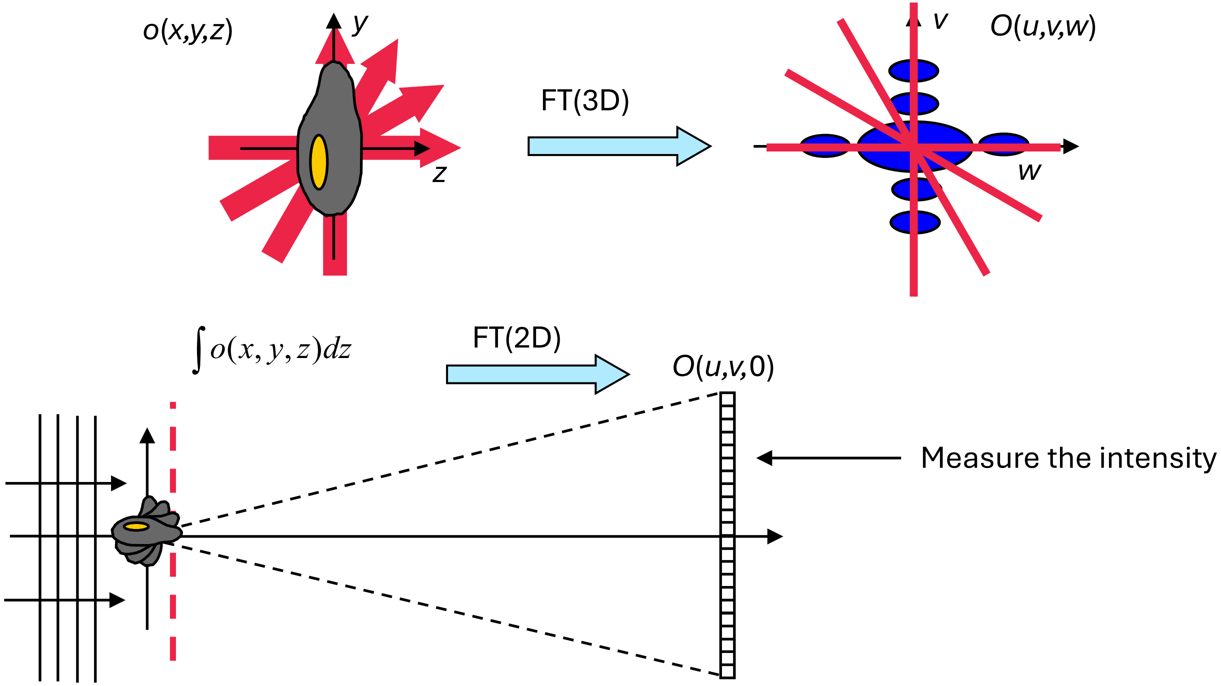

Scattering from a 3D object

For elastic scattering each scattered angle is produced by a particular grating

Bragg's law provides the mapping relation between the intensity in the detector plane and the 3D Fourier transform of the object

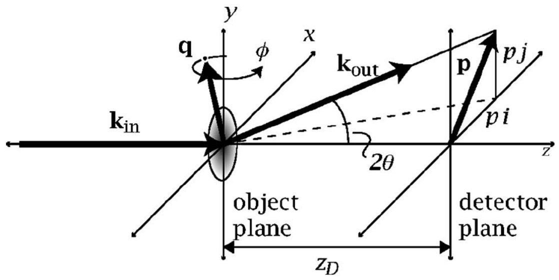

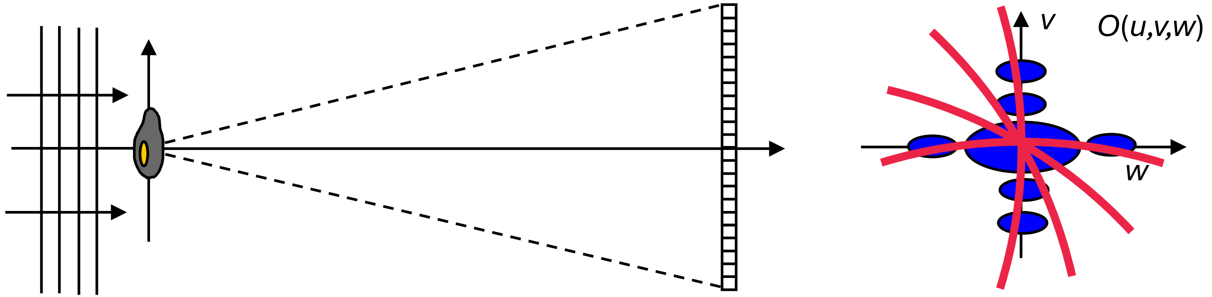

Each intensity measurement maps to a spherical shell on the 3D Fourier transform

Chapman *et al.* J. Opt. Soc. Am. A 23, 1179 (2006)

The pyramid test object

50 nm diameter gold spheres on a pyramidal indentation on silicon nitride membrane

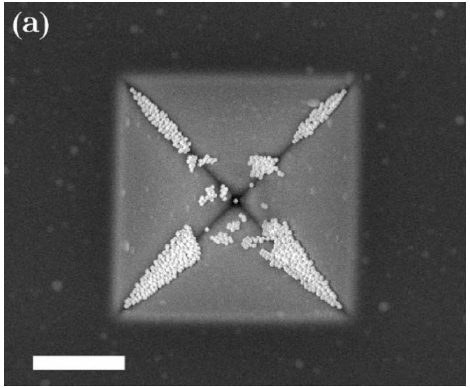

SEM image, surface sensitive only

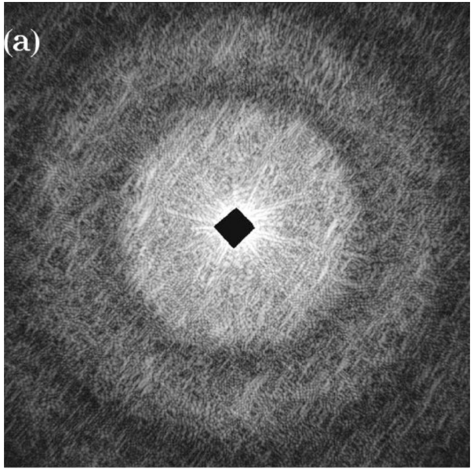

Measured diffraction pattern

10+ exposures to accommodate large dynamic range

H. N. Chapman *et al.*, J. Opt. Soc. Am. A 23, 1179 (2006)

Cuts through 3D Fourier intensity

Data voids from beam stop and large rotation increments

Missing wedge from limited range of rotations

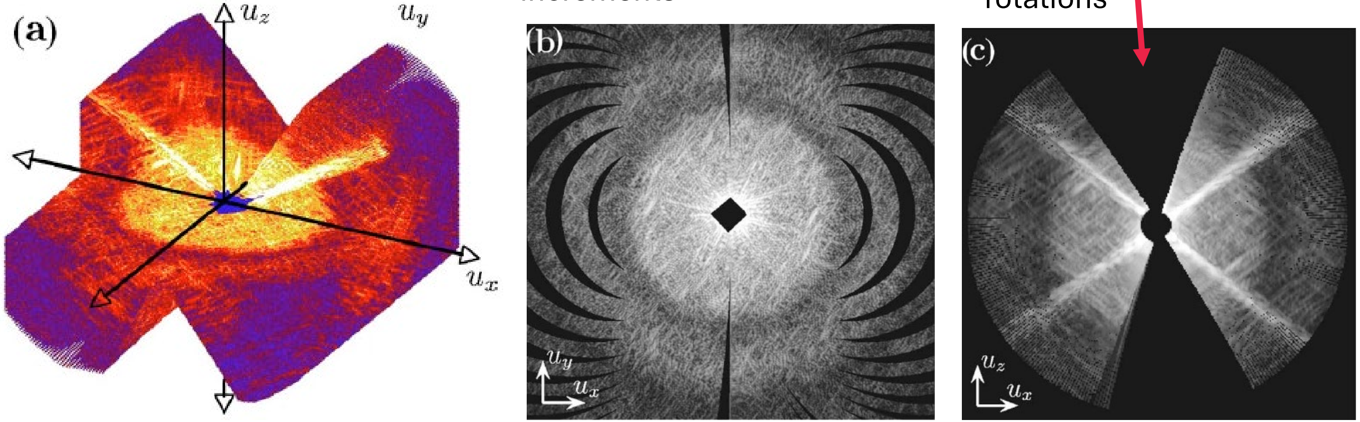

Total integrated exposure ~ 3.2 hours

H. N. Chapman et al., J. Opt. Soc. Am. A 23, 1179 (2006)

3D reconstruction

Phase retrieval algorithm was used to iteratively interpolate gaps in the data

Final resolution ~ 10x10x50 nm   (missing wedge)

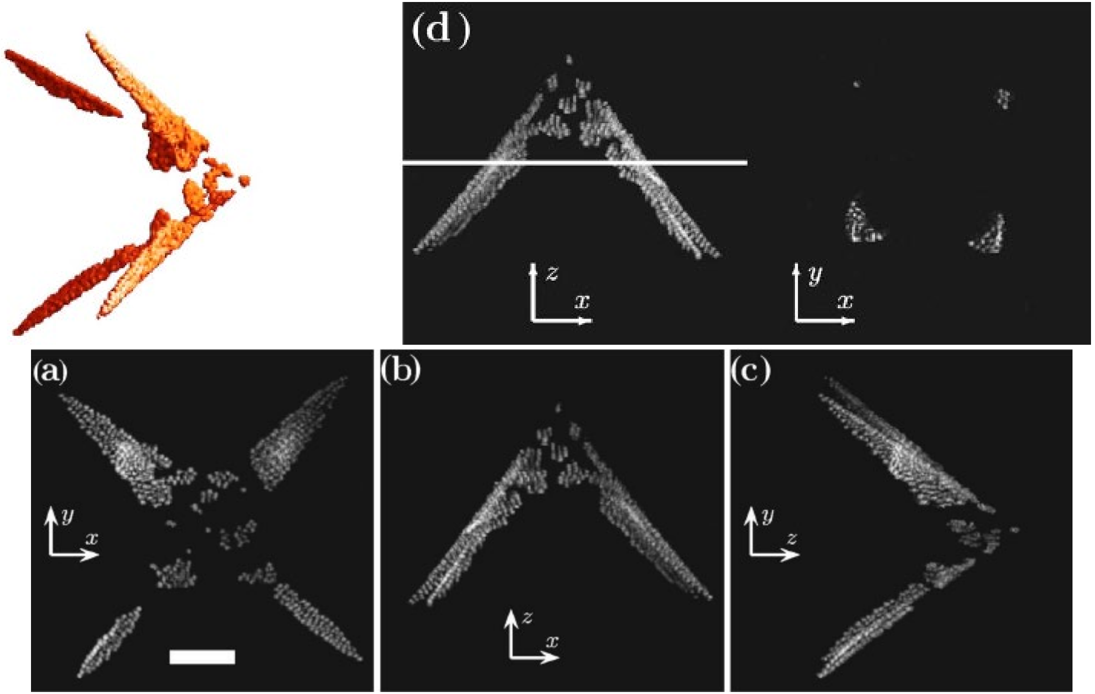

H. N. Chapman et al., "High-resolution ab initio three-dimensional x-ray diffraction microscopy," J. Opt. Soc. Am. A 23, 1179-1200 (2006)

3D CDI in routine use at ID10 of ESRF

Metal-coated monodisperse polymer spheres

Resolution better than 20 nm

Micro-composite of PMMA, Ni, Au, and SiO_2

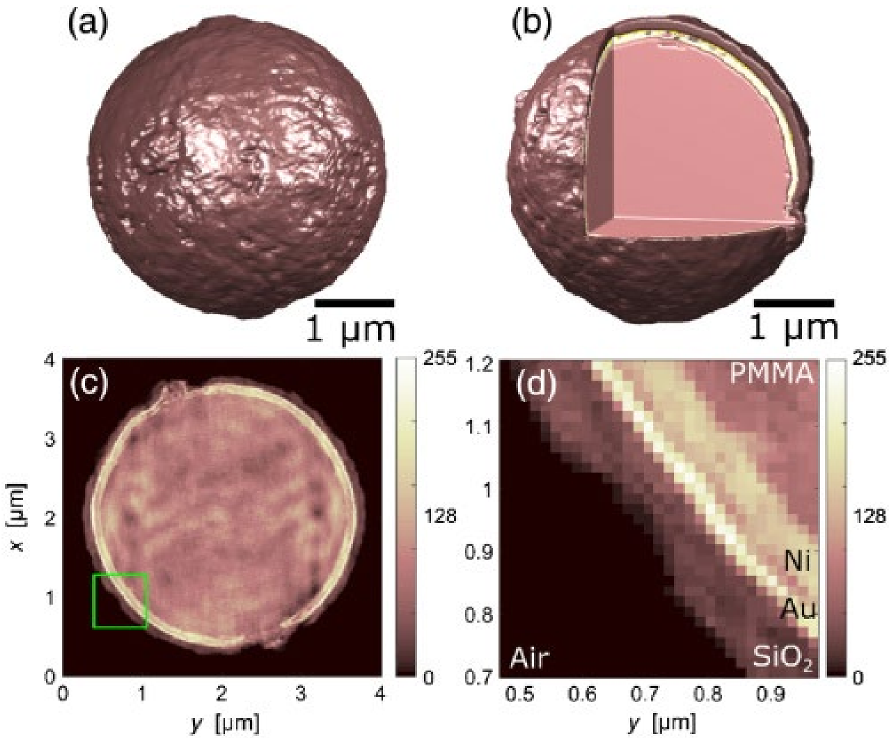

E. T. B. Skjønsfjell et al., J. Opt. Soc. Am. A **35**, A7 (2018)

Phase retrieval with a support constraint (CDI)

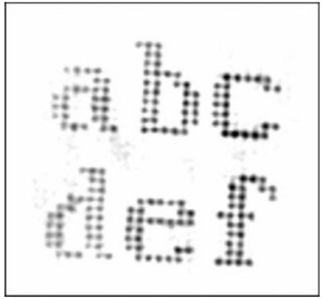

J. Miao et al., Nature **400**, 342 (1999)

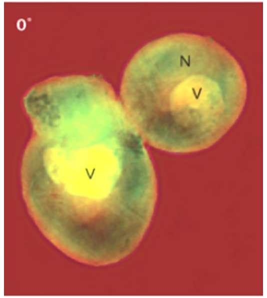

Specifically labeled freeze-dried yeast cell

J. Nelson *et al.*, PNAS **107**, 7235 (2010)

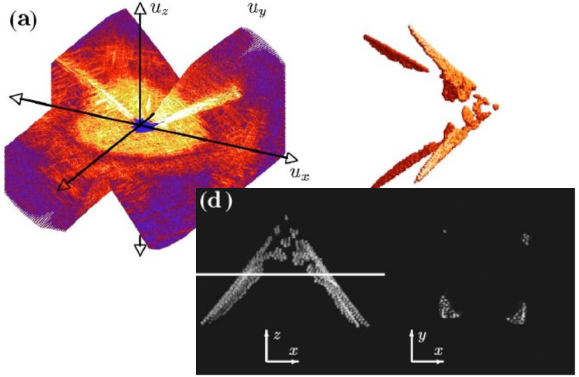

H. N. Chapman *et al.*, J. Opt. Soc. Am. A **23**, 1179 (2006)

Some limitations include

- Occasional stagnation
- Field of view limited by detector pixel
  (e.g. cSAXS@6.2 keV ~ 4 microns)
- Isolated sample (missing wedge)

$$fov = \frac{\lambda z}{2\Delta}$$

Phase retrieval with a support constraint (CDI)

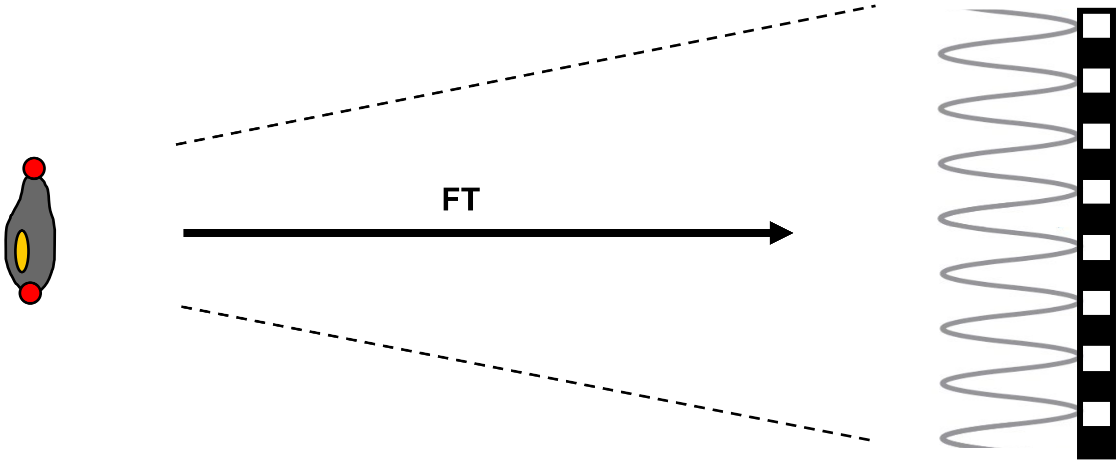

Some limitations include
- Occasional stagnation
- Field of view limited by detector pixel
  (e.g. cSAXS@6.2 keV ~ 4 microns)
- Isolated sample (missing wedge)

$$fov = \frac{\lambda z}{2\Delta}$$

Phase retrieval with a support constraint (CDI)

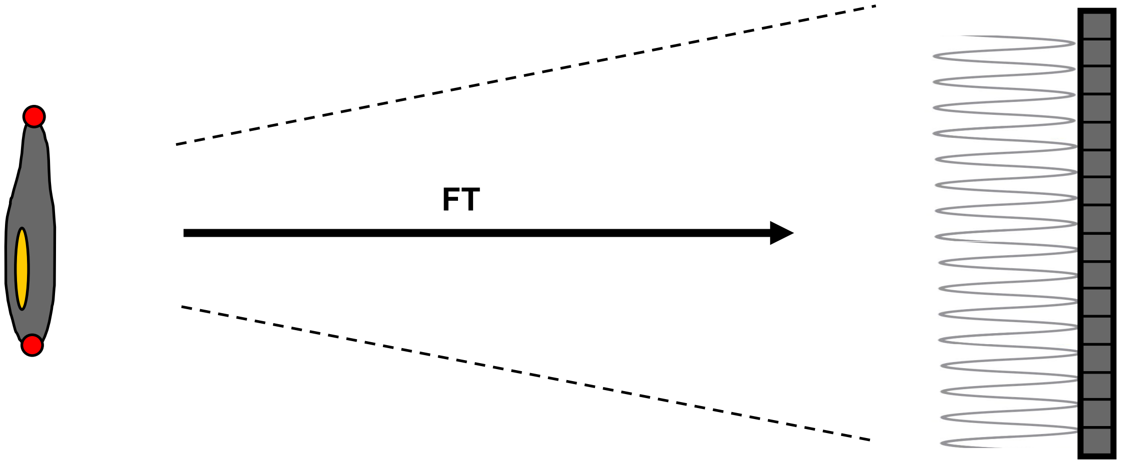

Some limitations include

- Occasional stagnation
- Field of view limited by detector pixel
  (e.g. cSAXS@6.2 keV ~ 4 microns)
- Isolated sample (missing wedge)

$$fov = \frac{\lambda z}{2\Delta}$$

Ambiguities in CDI

PSI

EPFL

Inherent ambiguities exist in CDI reconstructions. These are functions that can take arbitrary values → They are not constrained by the data

$$f(x, y) \rightarrow F(u, v)$$

$$f(x, y)\exp(ia) \rightarrow F(u, v)\exp(ia)$$

$$f(x-b, y) \rightarrow F(u, v)\exp(-i2\pi bu)$$

$$f^*(-x, -y) \rightarrow F^*(u, v)$$

if support is symmetric
either one could appear

Measure $|F(u, v)|^2$

$$f(x, y)\exp(i2\pi cx) \rightarrow F(u-c, v)$$

They are all successful reconstructions, but should be aware of them for interpretation of the reconstructions

Twin-image problem – Numerical simulation

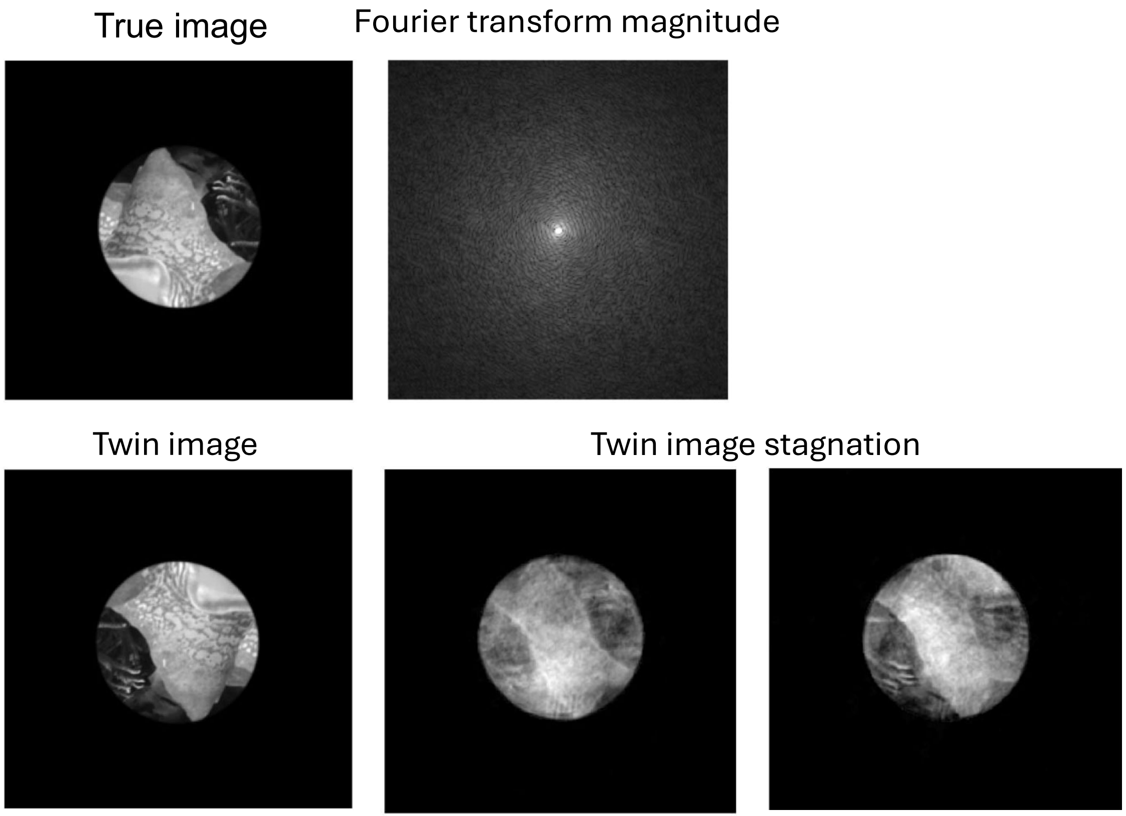

M. Guizar-Sicairos and J. R. Fienup, “Understanding the twin-image problem in phase retrieval,” J. Opt. Soc. Am A 29, 2367 (2012)

Outline

X-ray imaging

The phase problem (CDI)

- Ptychography

Ultrafast X-ray imaging with free-electron lasers

Ptychography

Resolving ambiguities of CDI
3D ptychography

Ptychography (transverse translation diversity)

Moving the sample with respect to a known illumination pattern can provide suitably diverse measurements

Makes phase retrieval more robust to stagnation, noise and ambiguities

Allows for extended samples, resolution is finer than the illumination size and scanning step

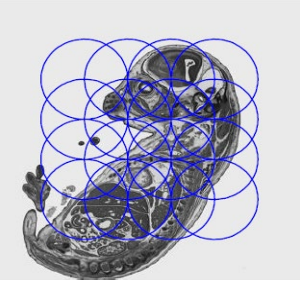

Complex-valued reconstruction

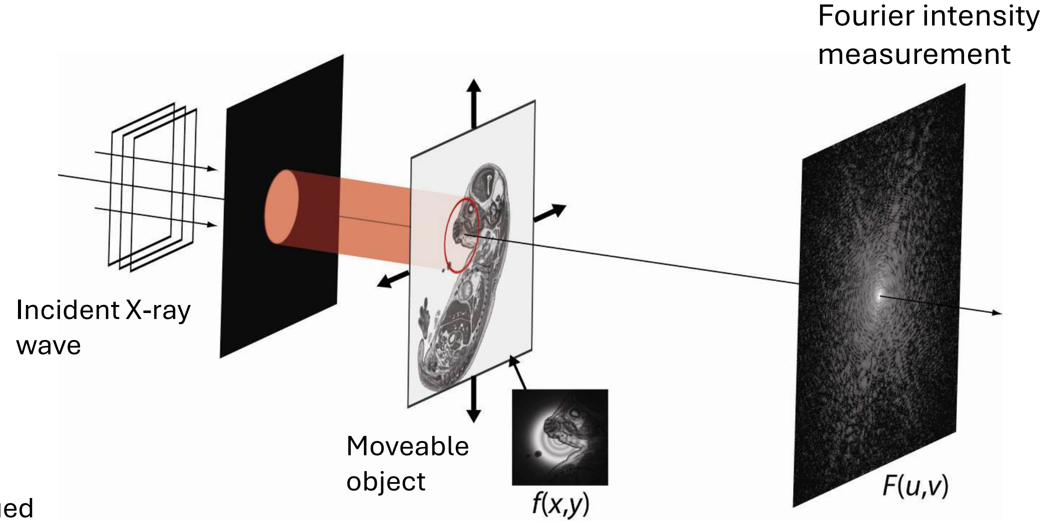

Overlap in the fields breaks the twin-image ambiguity

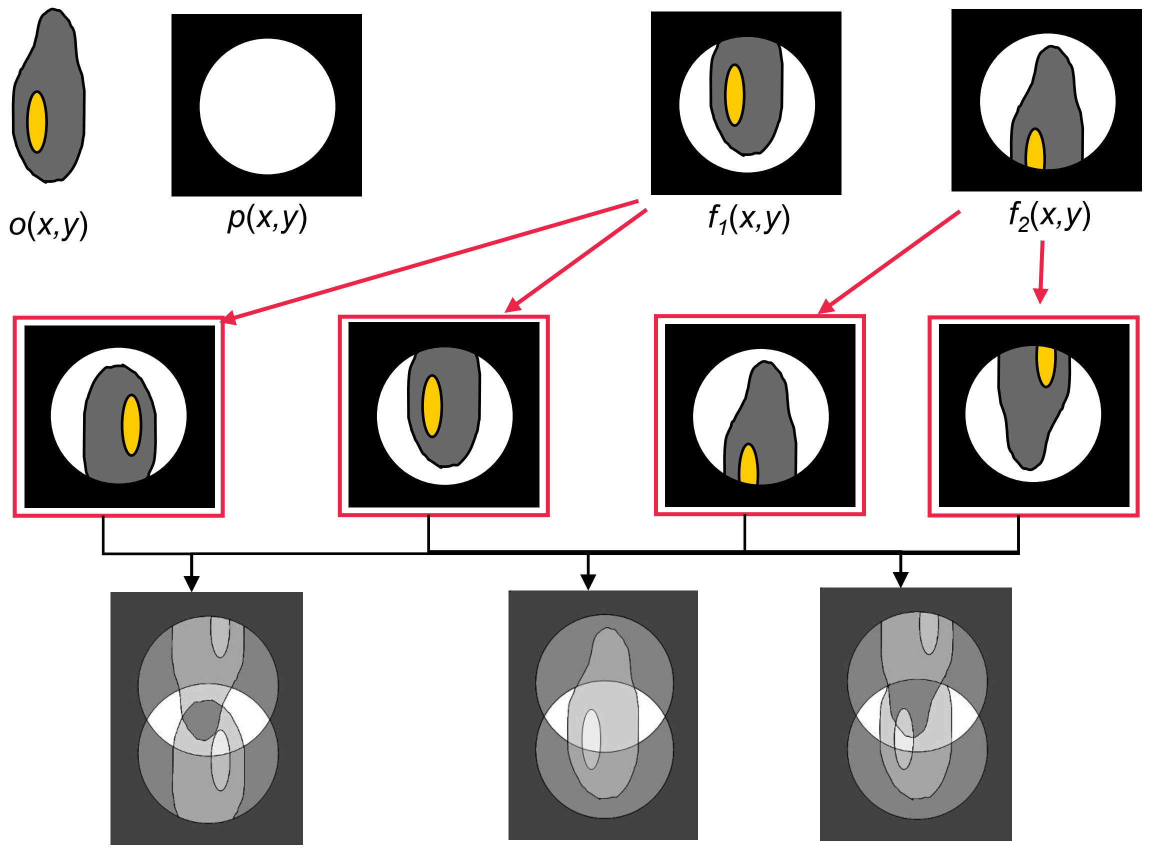

Imaging throughput – The Eiger self portrait

Sample 5 mm downstream of focus
Beam at sample ~ 10 microns
Scanning average step 3.5 microns

Eiger as sample and detector

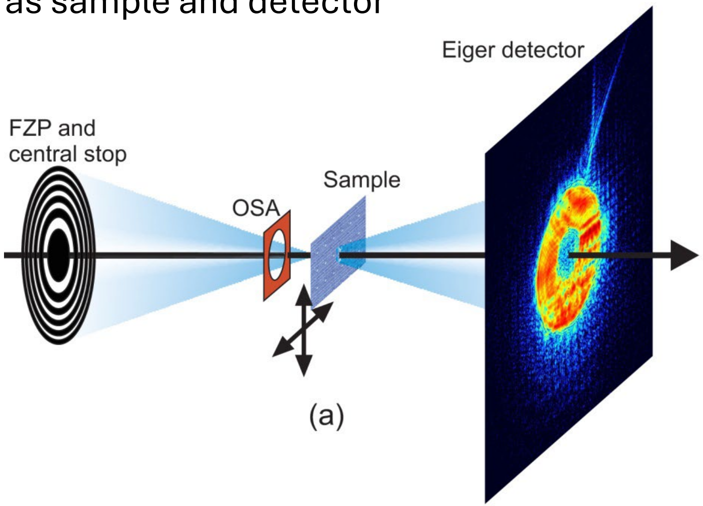

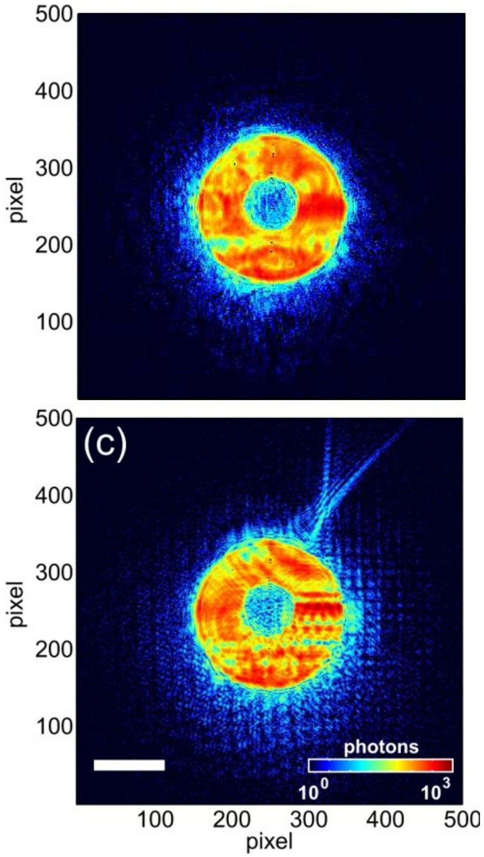

M. Guizar-Sicairos *et al.*, Opt. Express **22**, 14859 (2014)

Imaging throughput – The Eiger self portrait

98.4 Mpixel (13,028 x 7,556)
Resolution 41 nm, 38.4 nm pixel
> 25,000 resolution elements / second
40 microsecond per resolution element

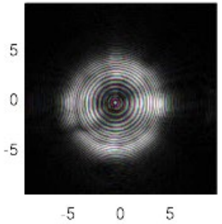

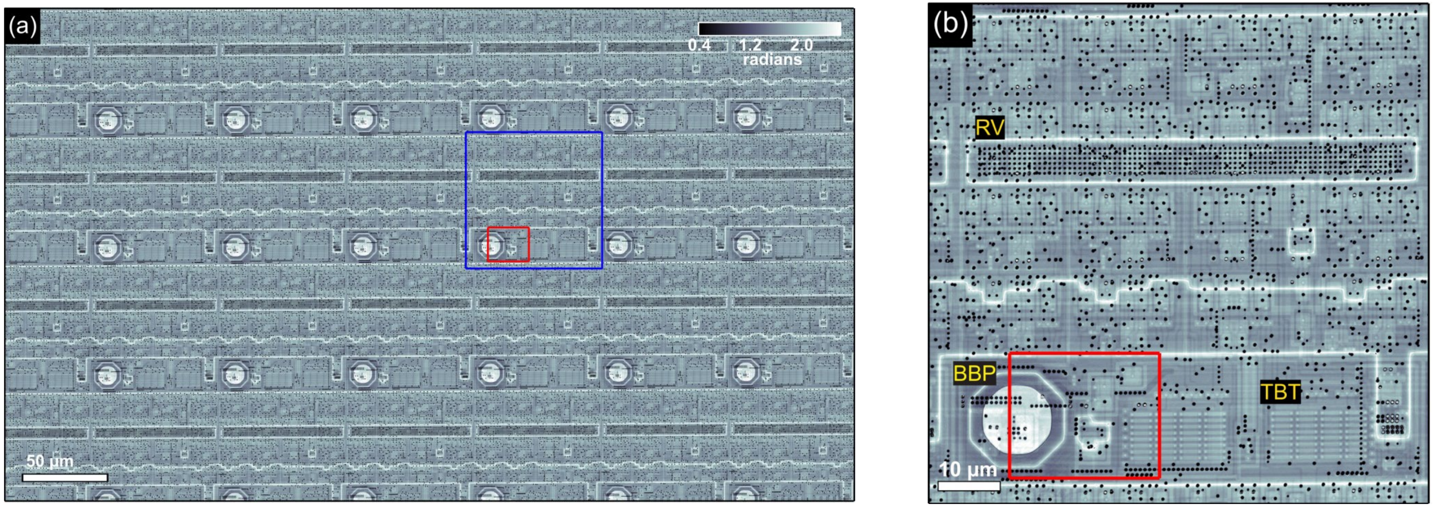

M. Guizar-Sicairos *et al.*, Opt. Express **22**, 14859 (2014)

Imaging throughput – The Eiger self portrait

98.4 Mpixel (13,028 x 7,556)
Resolution 41 nm, 38.4 nm pixel
> 25,000 resolution elements / second
40 microsecond per resolution element

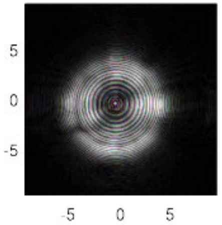

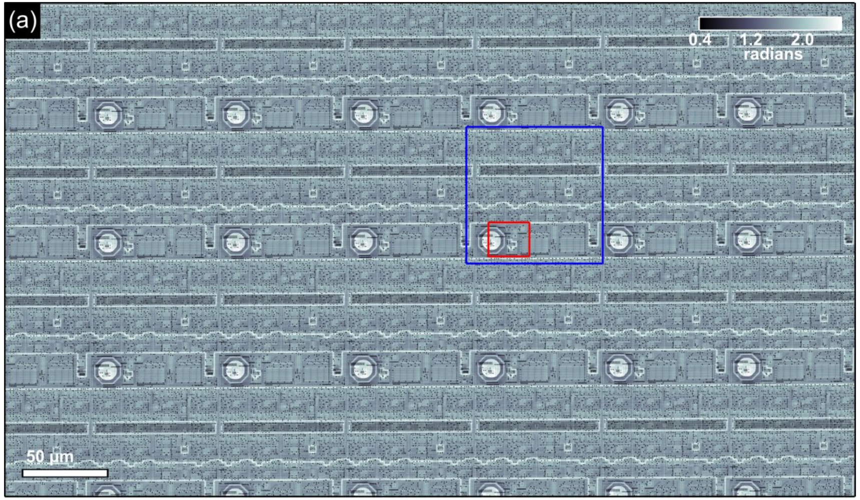

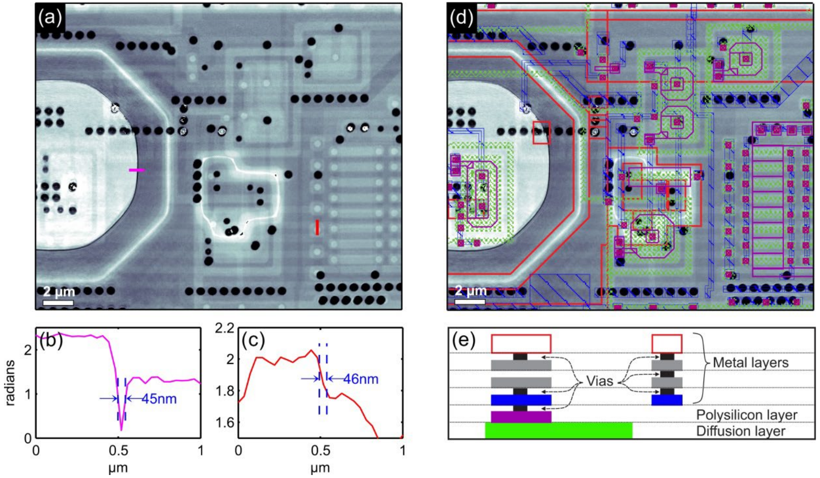

M. Guizar-Sicairos *et al.*, Opt. Express **22**, 14859 (2014)

PtychoShelves

A versatile high-level framework for high-performance analysis of ptychographic data

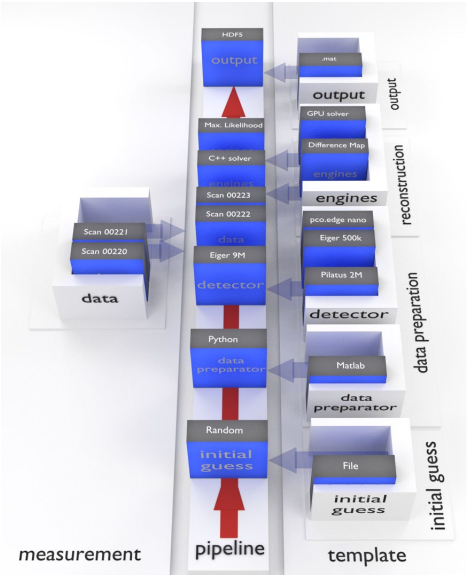

Modular framework: Matlab, C++, GPU Cuda

Distributed: MPI, multiple GPU cards, minimal memory synchronization

High-performance reconstruction engines (Scientific computing)

Batch processing and online reconstructions

SLS (cSAXS, SIM), APS, SOLEIL, Cornell Univ. (electron ptychography)

Mutliple reconstruction algorithms can be concatenated

Multislice, mixed coherent modes, modal probe relaxation, sharing reconstructions between scans, position refinement, global position geometry refinement

K. Wakonig,* H.-C. Stadler, M. Odstrčil, E. H. R. Tsai, A. Diaz, M. Holler, I. Usov, J. Raabe, A. Menzel, and M. Guizar-Sicairos*, J. Appl. Cryst. **53**, 574 (2020)

Ptychographic X-ray computed tomography (PXCT)

Phase of reconstruction corresponds to the integrated x-ray phase-shift

Combined with sample rotation and computed tomography algorithms the real part of the 3D index of refraction can be reconstructed

$$t(x,y,\theta) = \exp\left\{\frac{i2\pi}{\lambda}\int[n(\mathbf{r}')-1]dz\right\}$$

$$n(\mathbf{r}) = 1-\delta(\mathbf{r})+i\beta(\mathbf{r})$$

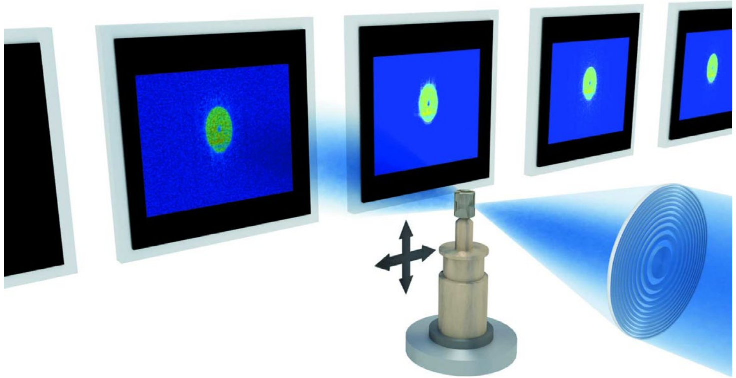

K. Wakonig,* H.-C. Stadler, M. Odstrčil, E. H. R. Tsai, A. Diaz, M. Holler, I. Usov, J. Raabe, A. Menzel, and M. Guizar-Sicairos*, J. Appl. Cryst. **53**, 574 (2020)

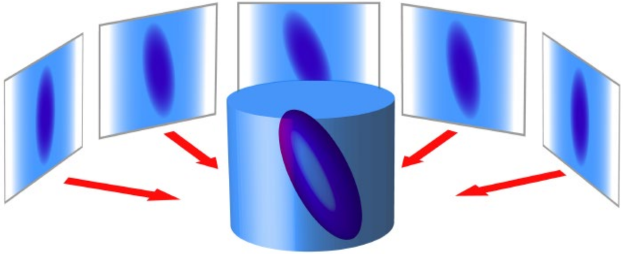

M. Guizar-Sicairos et al., Opt. Express **19**, 21345 (2011)

Basics of computed tomography

Imaging sections of the interior without physical sectioning

Starting from projections, line integrals from different orientations,

how to reconstruct the object?

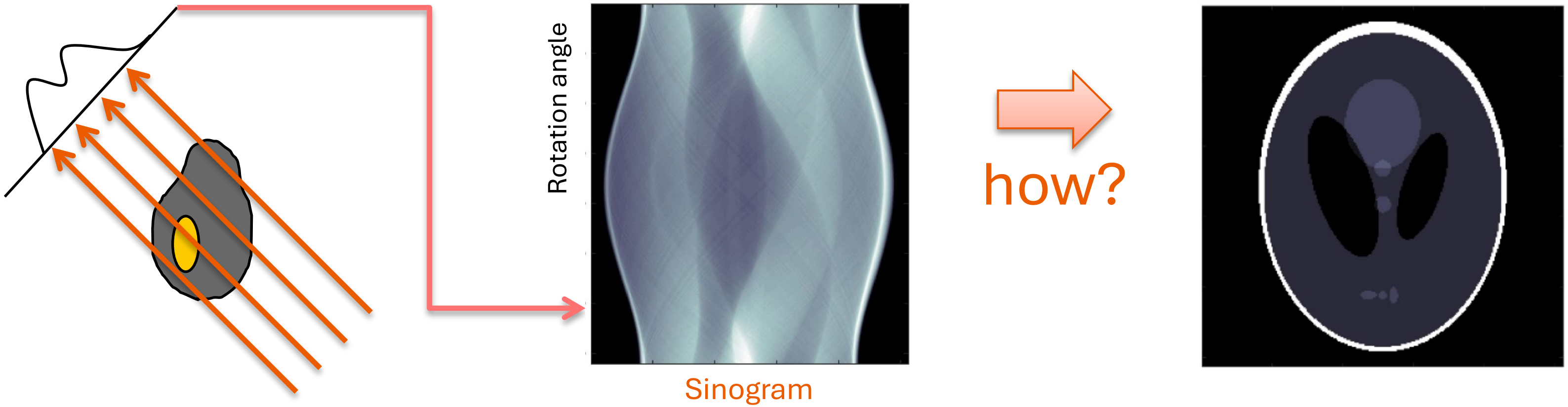

Projections measured for all possible orientations

Filtered back-projection

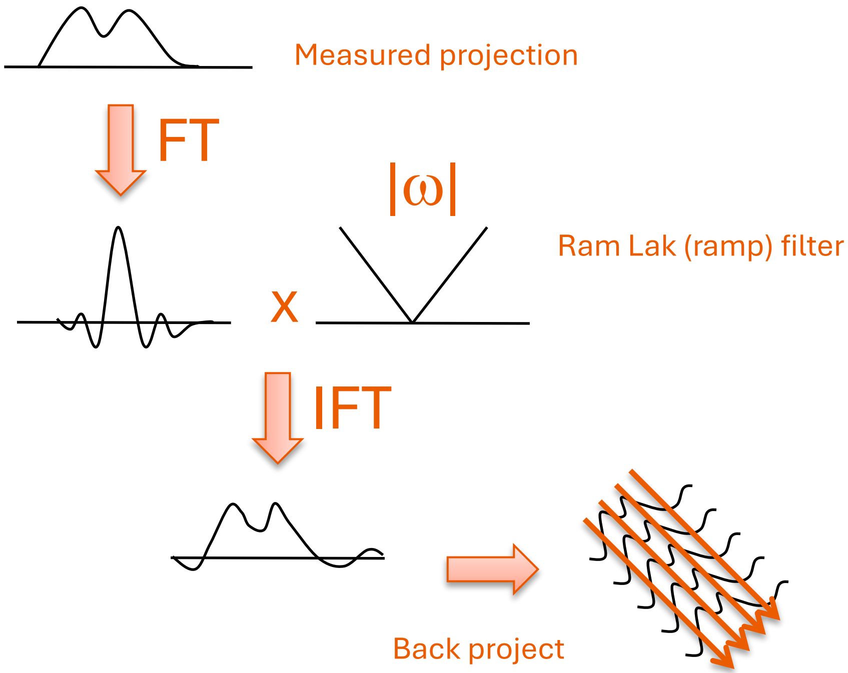

$$\mu(x,y)=\int_0^{\pi} d\theta \int_{-\infty}^{\infty} \tilde{P}(\omega,\theta)\left|\omega\right| e^{j2\pi\omega t}\, d\omega$$

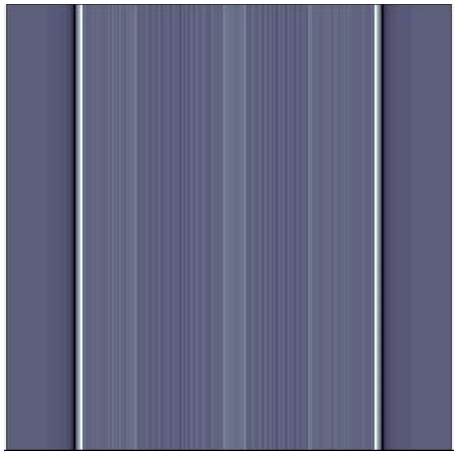

Filtered back-projection

$$\mu(x,y)=\int_{0}^{\pi}d\theta\int_{-\infty}^{\infty}\tilde{P}(\omega,\theta)\left|\omega\right|e^{j2\pi\omega t}\,d\omega$$

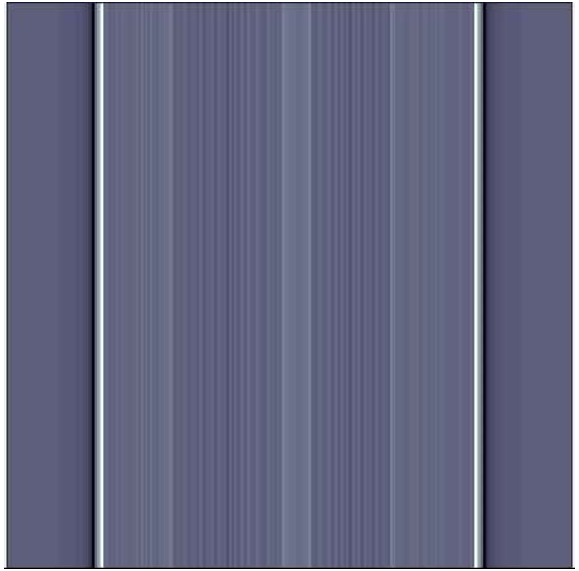

FT

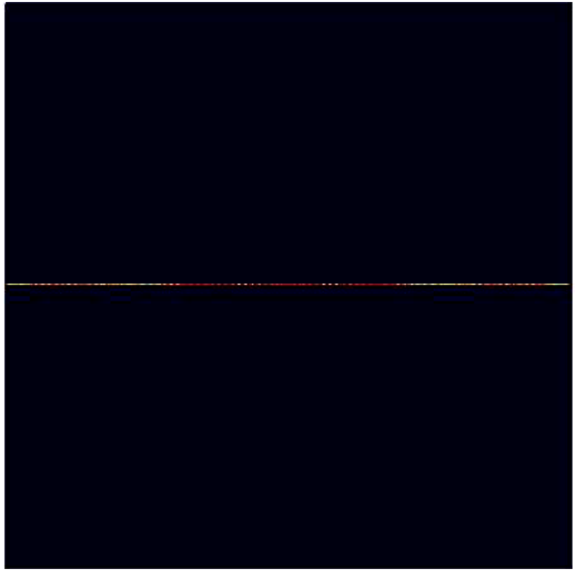

OMNY: The cryo-stage instrument

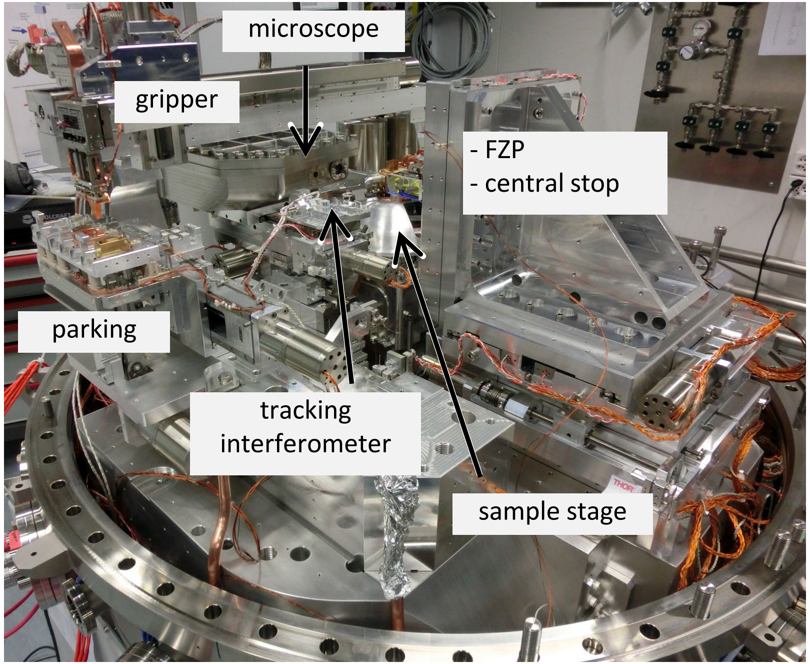

M. Holler, J. Raabe, and engineer team at PSI

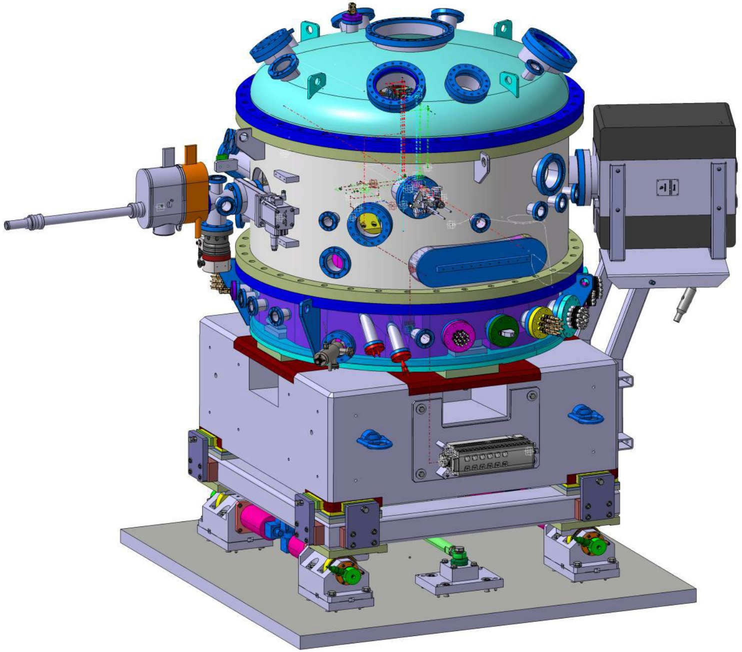

M. Holler *et al.*, Rev. Sci. Instrum. **89**, 043706 (2018)

OMNY: The cryo-stage instrument

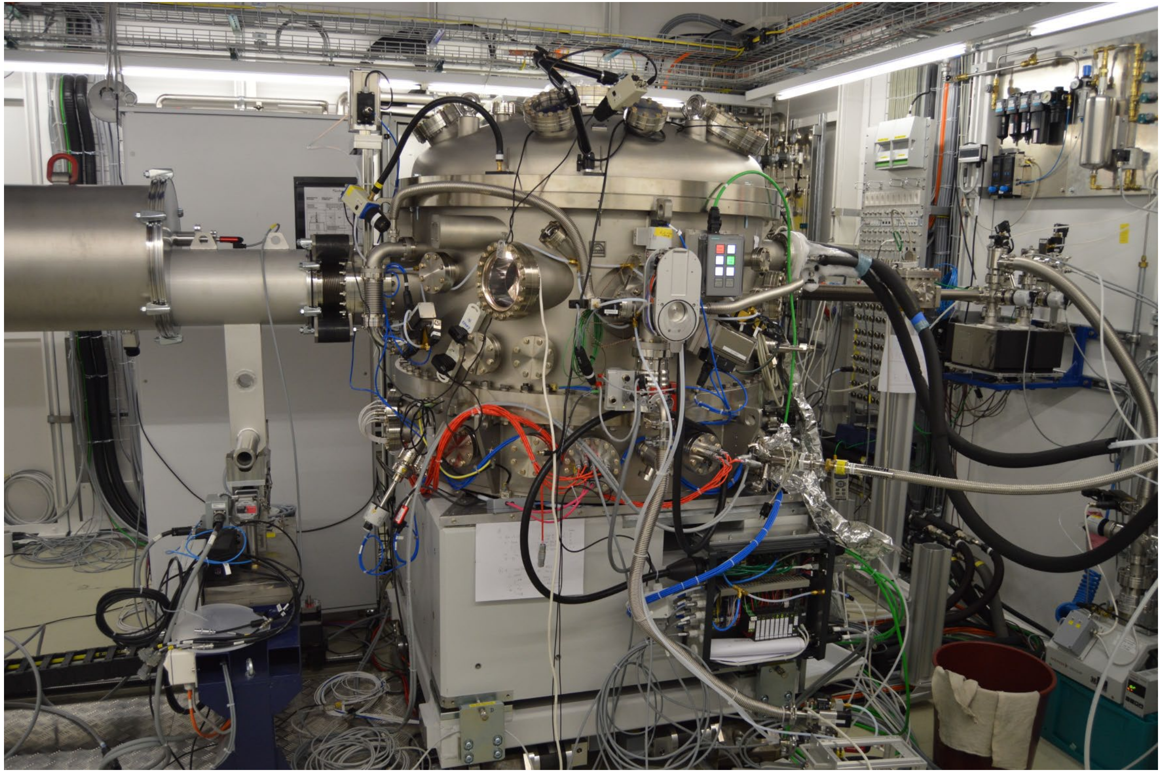

First visit at the beamline June 3-15, 2015 for commissioning and measurements

Unstained human brain tissue

PSI
EPFL

Brain region: substantia nigra pars compacta
Chemically fixed, hydrated, unstained

healthy

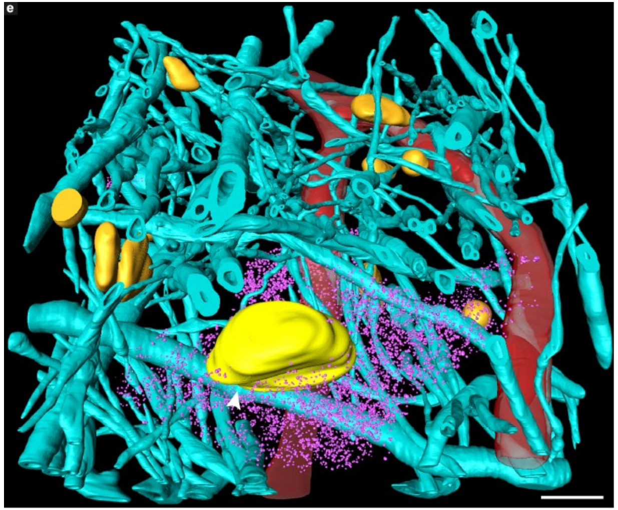

5 specimens imaged from a healthy individual as control

Parkinson-affected

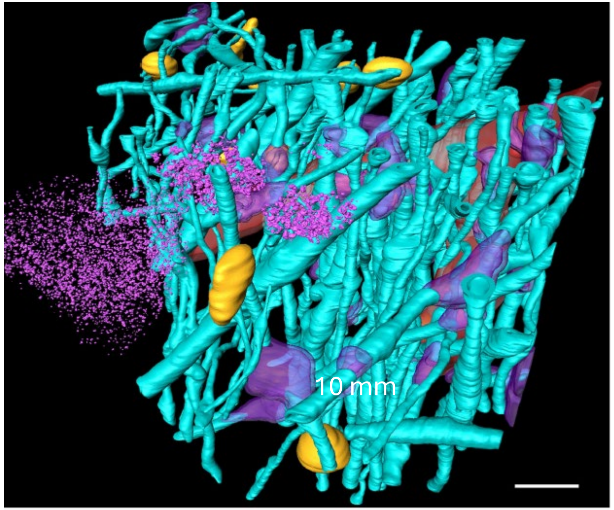

4 specimens imaged from a Parkinson-affected individual

Myelinated axons
Swellings along axons
Cell nuclei
Neuromelanin-containing organelles
Blood vessels
Blood cells

Tran, H. T. *et al*. Front. Neurosci. **14**:570019.

Unstained human brain tissue

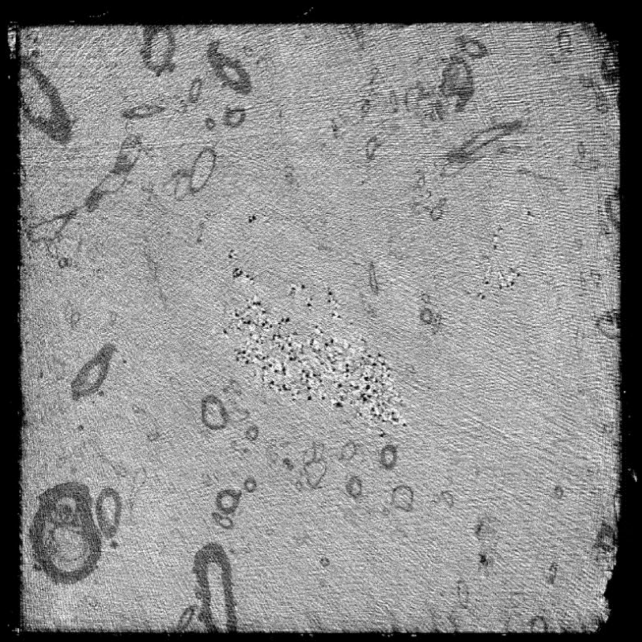

25 µm

Tran, H. T. et al.
Front. Neurosci. 14:570019.

Myelinated axons
Swellings along axons
Cell nuclei
Neuromelanin-containing organelles
Blood vessels
Blood cells

Nanoscale 3D imaging

Combine ptychography with sample rotation

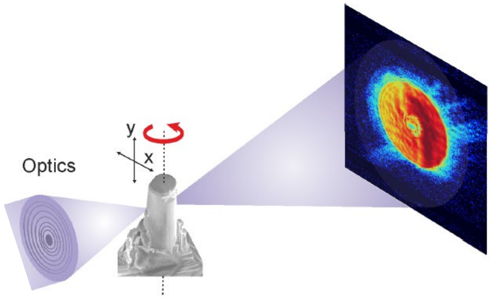

Image modified from Donnelly *et al*. Nature 547, 328 (2017)

Ptychographic X-ray computed tomography (PXCT)

Dierolf *et al.* “Ptychographic X-ray computed tomography at the nanoscale,” Nature, **467** 436 (2010)

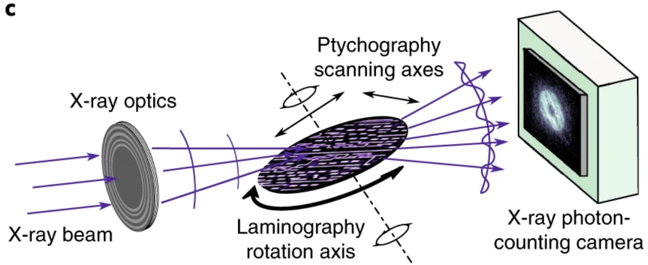

Ptychographic X-ray laminography (PyXL)

Holler *et al.*, “Three-dimensional imaging of integrated circuits with macro- to nanoscale zoom,“ Nat. Electron. **2**, 464 (2019)

Nanoscale 3D imaging – Metal connectome

Holler et al, Nat. Electron. 2, 464 (2019)

Integrated circuit (16 nm CMOS FinFET) at 20 nm resolution. Measurement in SLS, cSAXS.

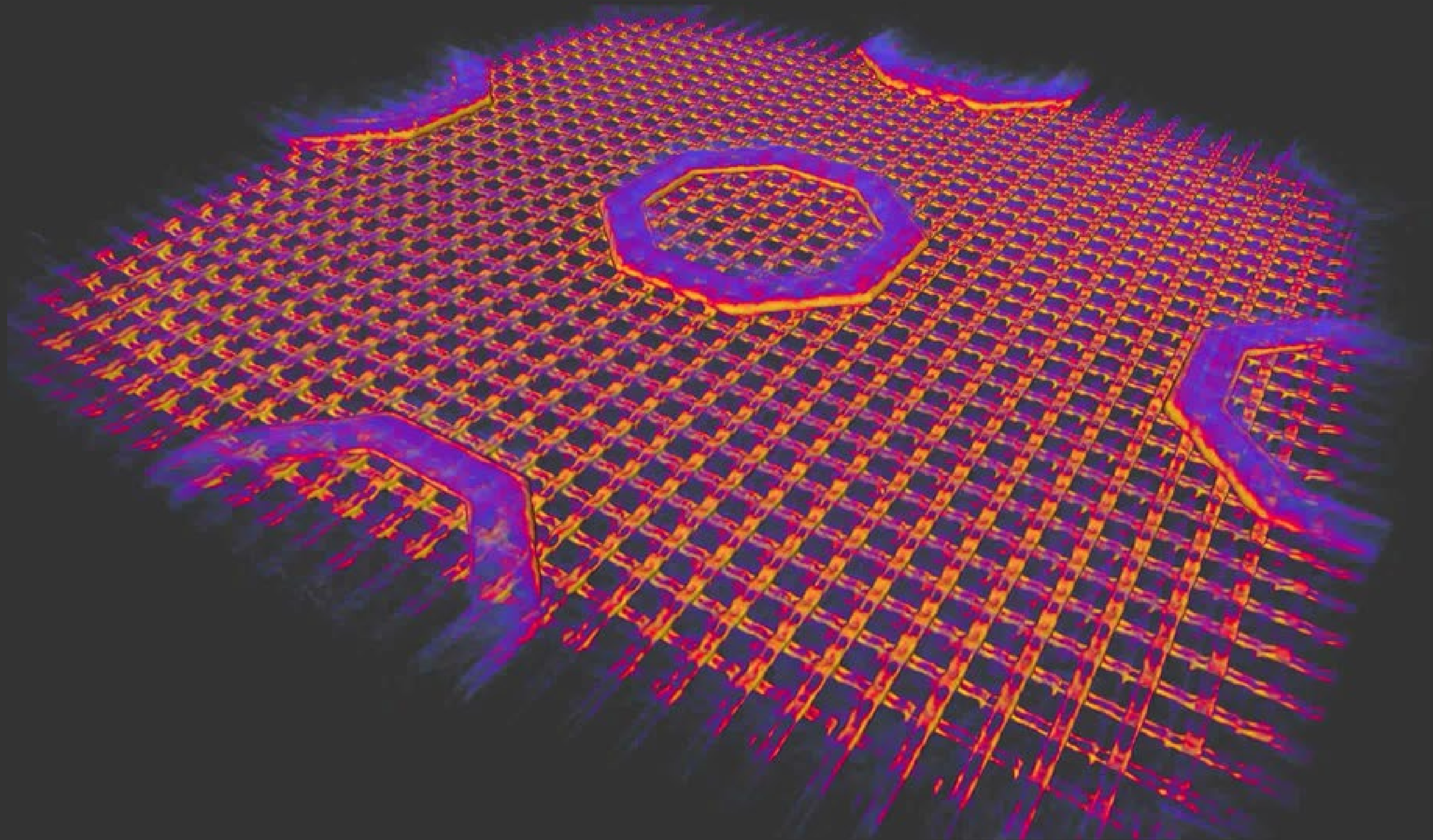

Laminography Nano Imaging (LamNI)

Integrated circuit

FOV 40x40 microns

20 nm resolution

Smallest gaps and metal connects ~30 nm

Laminography configuration also reduces streak artifacts

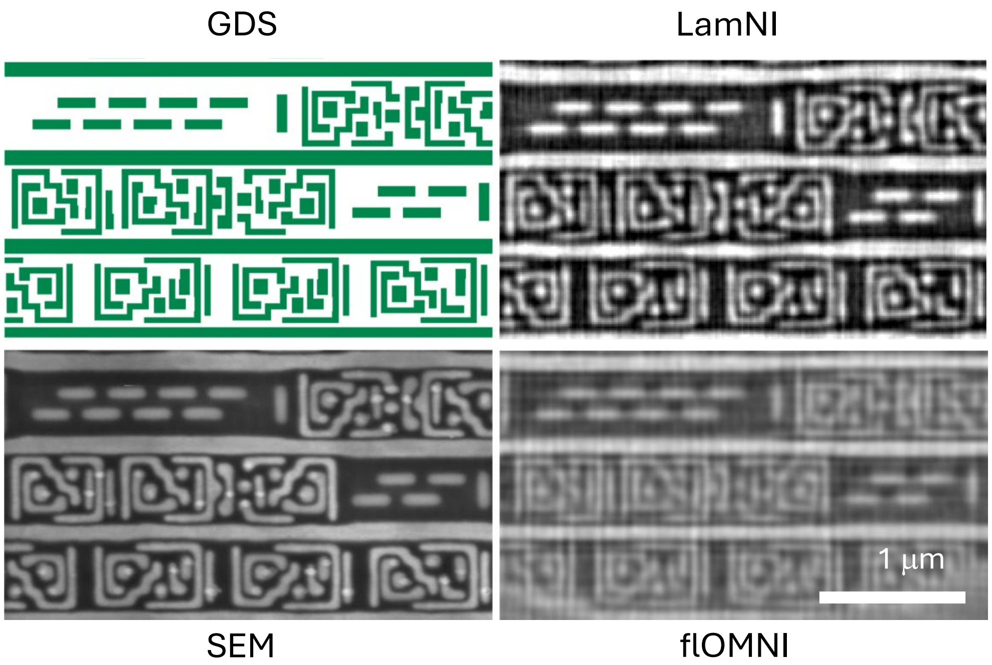

Holler et al, "Three-dimensional imaging of integrated circuits with macro- to nanoscale zoom," Nat. Electron. 2, 464 (2019)

Further reading

M. Guizar-Sicairos and P. Thibault, Physics Today **74,** 42 (2021). September 2021

History
Links to other techniques
Different ptychography flavours
Applications

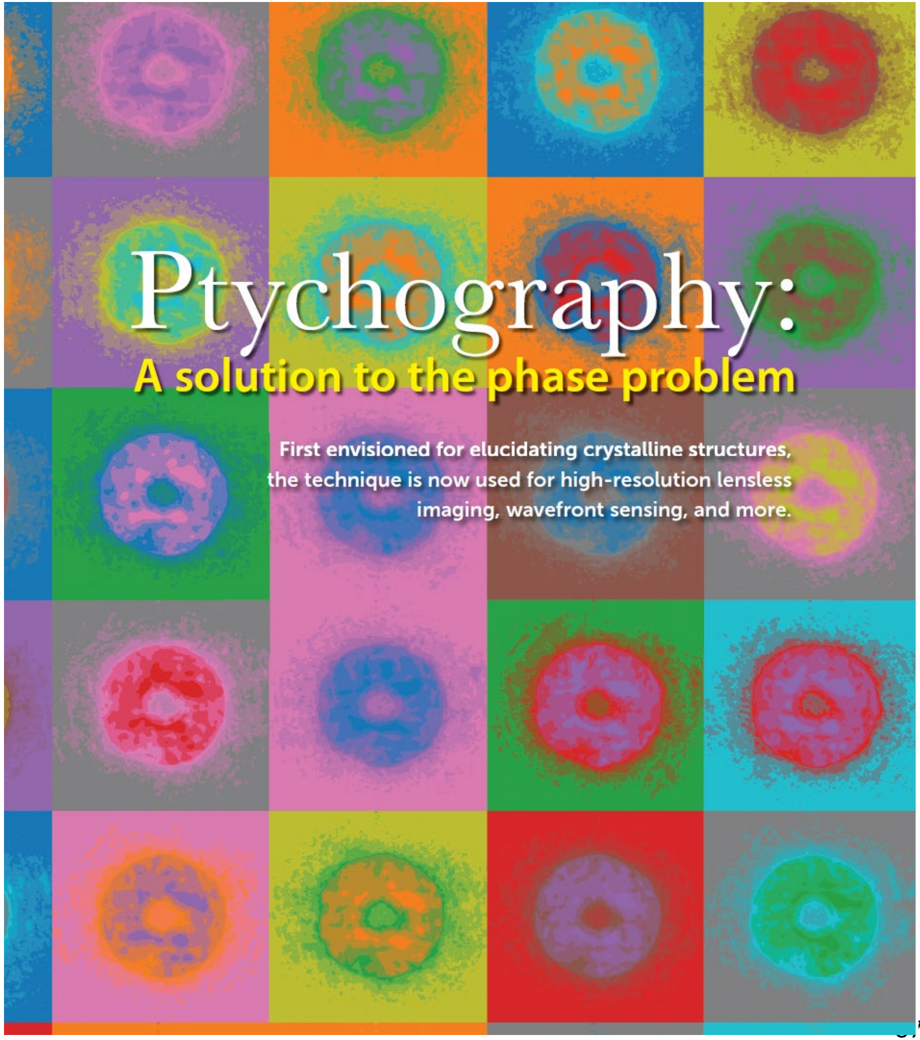

Resolution record in electron microscopy

Resolution record in electron microscopy

1948 – Holography invented (Dennis Gabor, Physics Nobel 1971)
1958 – Laser invented, Townes (Physics Nobel 1964) and Schawlow (Physics Nobel 1981) are mostly credited, but it's a complicated story
1969 – Ptychography is proposed for electron microscopy by Walter Hoppe

Instrumentation and coherence was not really ready for electron microscopy, and optical wavelengths already had good imaging techniques

Electron ptychography achieves atomic-resolution limits set by lattice vibrations

Back full circle – Ptychography was first conceived in 1969 by W. Hoppe for electron microscopy

Resolution **15 pm**
$PrScO_3$ sample with a thickness of **21 nm**
Column width of reconstruction limited by finite size of atoms (thermal fluctuations)
Ptycho overcomes lens aberrations and multiple scattering

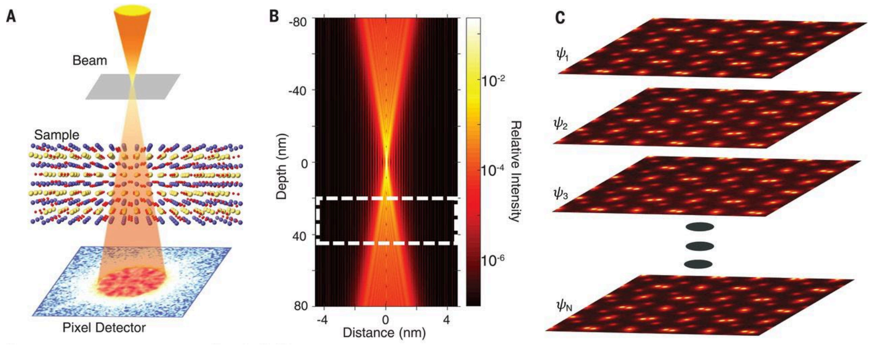

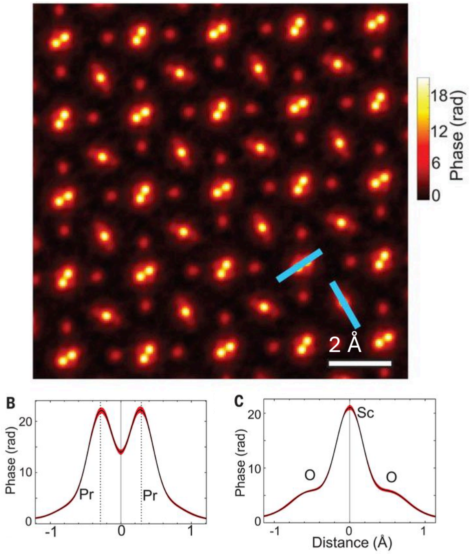

Praseodymium,Scandium

Z. Chen et al., Science 372, 826 (2021)

Collaboration with Prof. David Muller.

Electron ptychography achieves atomic-resolution limits set by lattice vibrations

Back full circle – Ptychography was first conceived in 1969 by W. Hoppe for electron microscopy

Resolution **<u>15 pm</u>**
$PrScO_3$ sample with a thickness of **<u>21 nm</u>**
Column width of reconstruction limited by finite size of atoms (thermal fluctuations)
Ptycho overcomes <u>lens aberrations and multiple scattering</u>

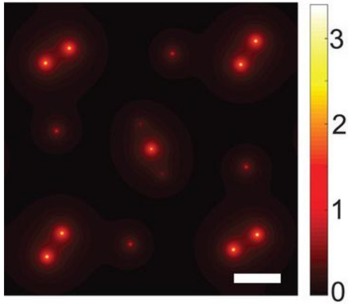

Electrostatic potential Simulated at 0 K

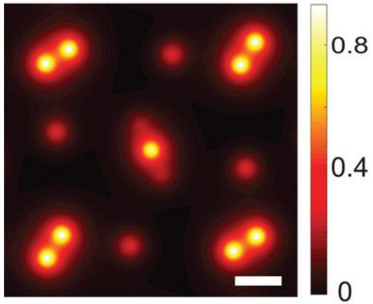

Simulated thermal broadening at 300 K

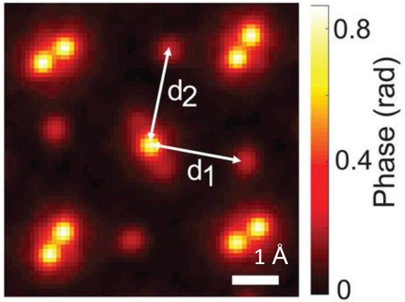

Experimental at 300 K

Z. Chen et al., Science 372, 826 (2021)

Collaboration with Prof. David Muller.

Resolution record in X-ray tomography

Pushing the limits of X-ray imaging resolution

A plateau/bottleneck in resolution was observed → increased statistics did not improve resolution

Fast short exposures at a fixed position revealed instabilities of the X-ray illumination

Tomas Aidukas

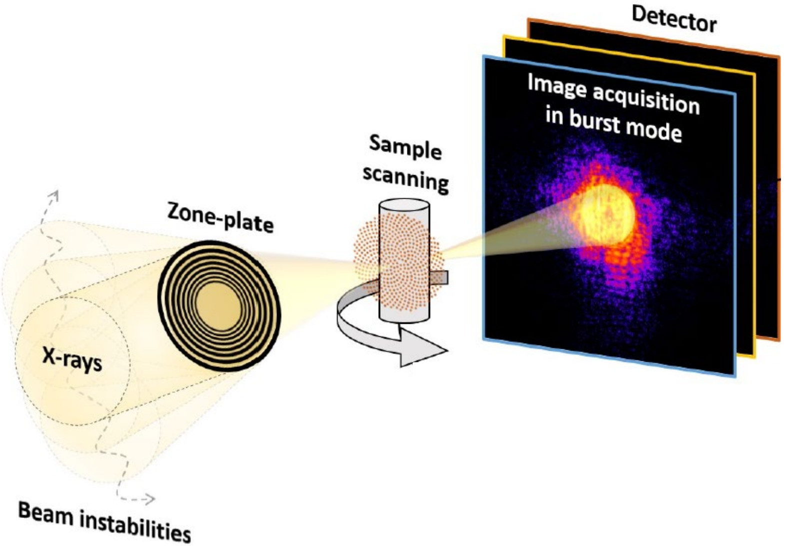

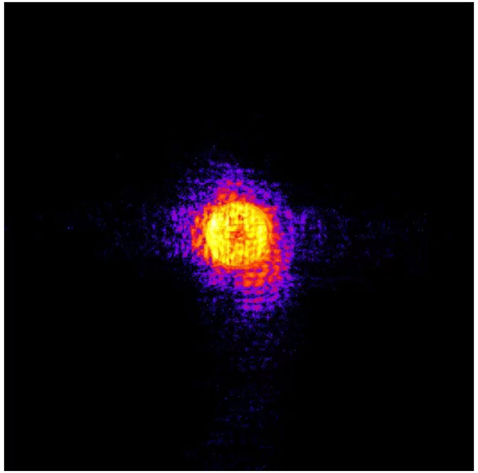

8 ms exposure time

Pushing the limits of X-ray imaging resolution

Higher photon statistics

Blurred diffraction patterns → lower SNR

Breaches assumption of constant illumination

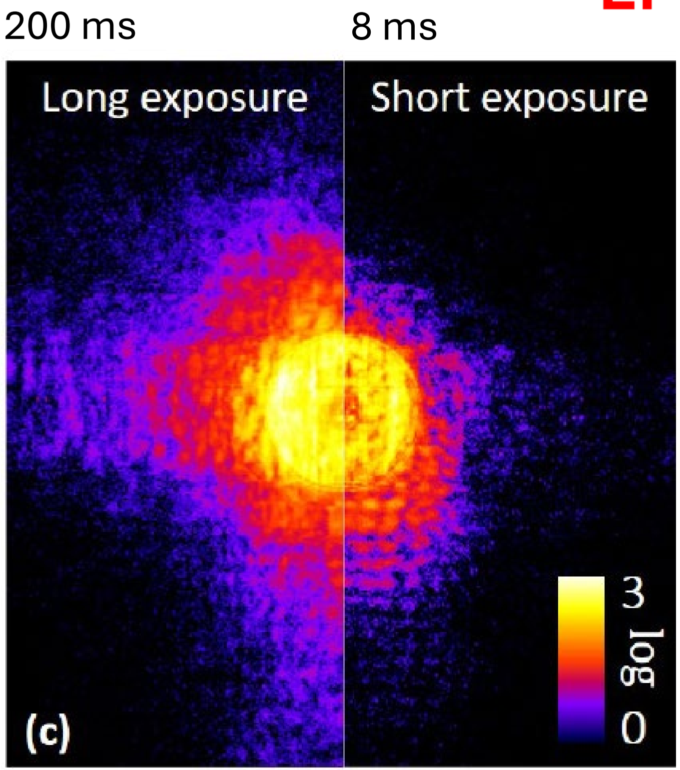

Burst ptychography

Many fast acquisitions per scanning point
Use ptychography position refinement to identify and average frames with similar positions → All data is used

Tomas Aidukas

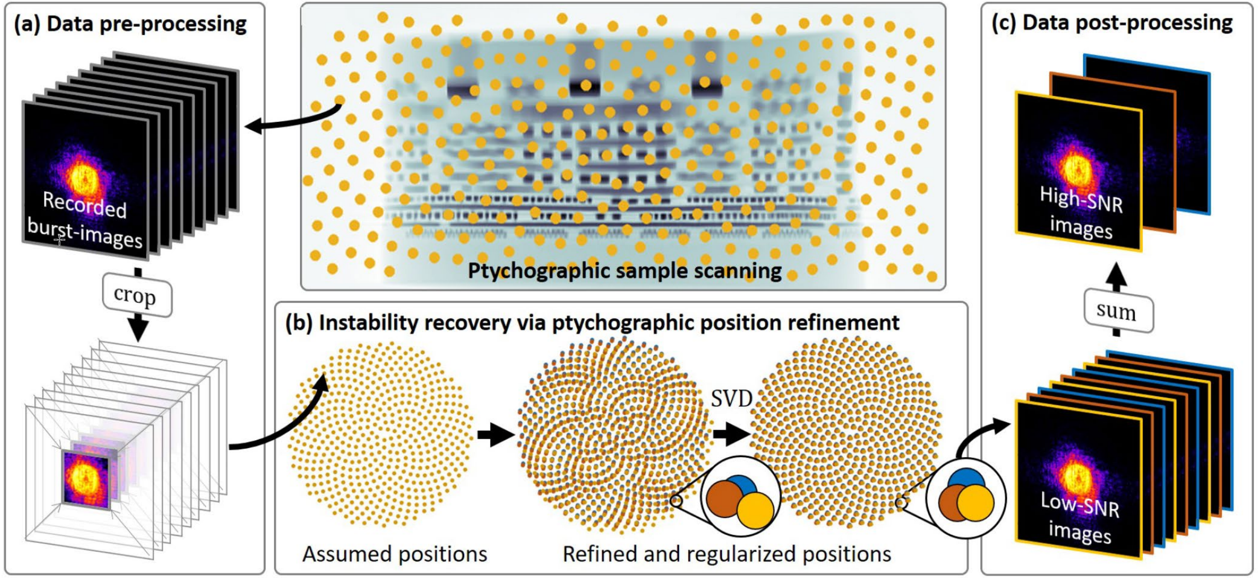

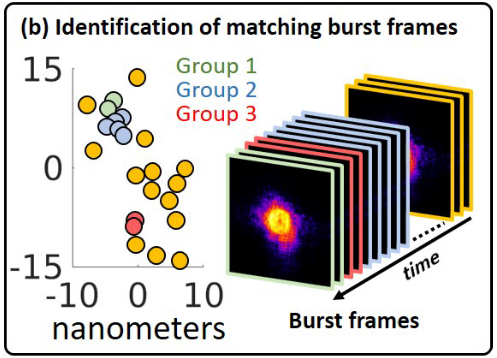

AMD Ryzen 5 5600G GPU IC

TSMC 7 nm node technology (measure of transistor density)

38 hour measurement @cSAXS beamline

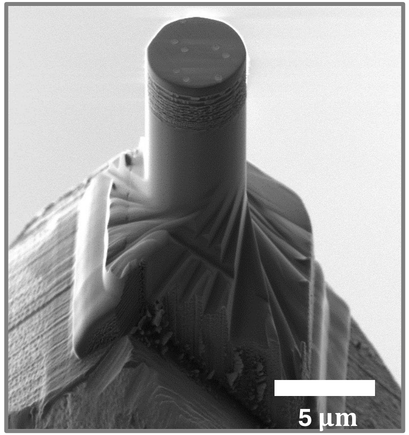

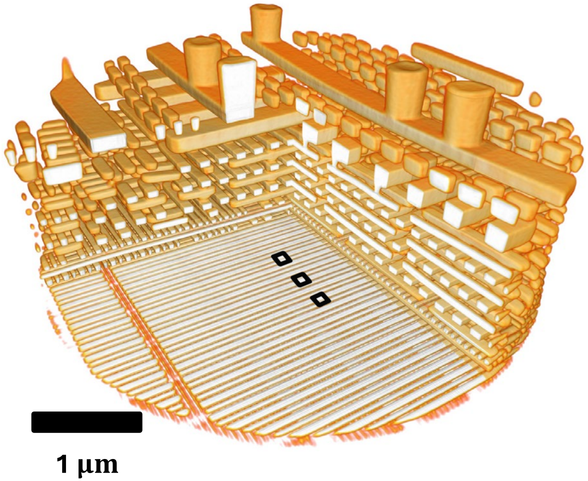

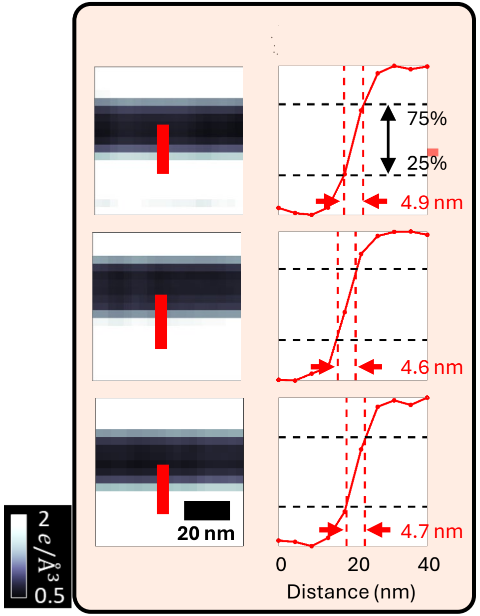

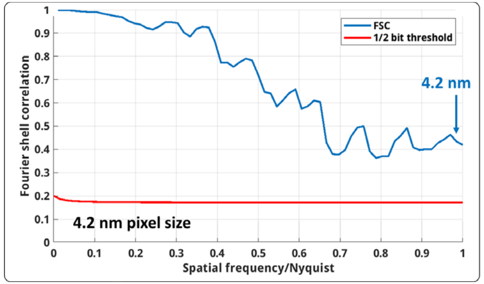

T. Aidukas, N. W. Phillips, A. Diaz, E. Poghosyan, E. Müller, A. F. J. Levi, G. Aeppli, M. Guizar-Sicairos, and M. Holler, "High-performance 4-nm-resolution X-ray tomography using burst ptychography," Nature **632**, 81 (2024)

Extended depth of field

We have not obtained good results with multi-slice ptychography in X-rays
→ Proper modeling of beam propagation through the sample
We get a complex-valued transmissivity → here we use filtered back-propagation instead of filtered back projection in the tomographic step

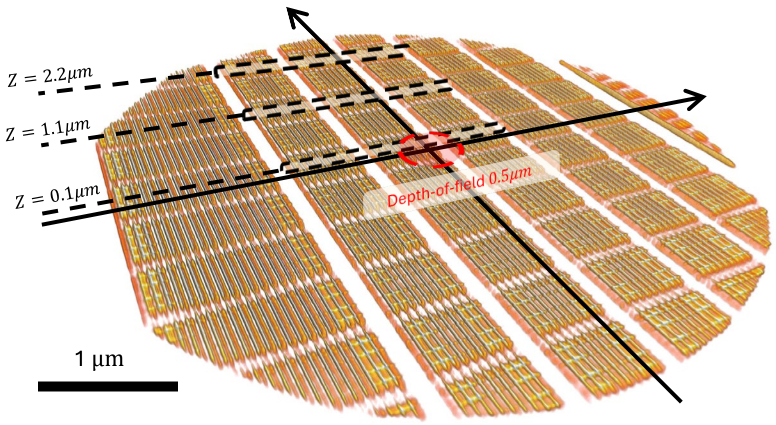

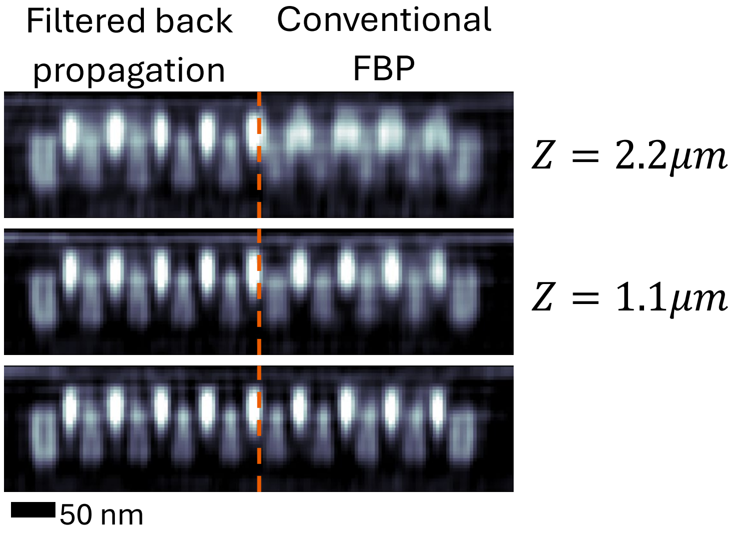

T. Aidukas, N. W. Phillips, A. Diaz, E. Poghosyan, E. Müller, A. F. J. Levi, G. Aeppli, M. Guizar-Sicairos, and M. Holler, "High-performance 4-nm-resolution X-ray tomography using burst ptychography," Nature **632**, 81 (2024)

The metal connectome – 4 nm resolution

PSI

EPFL

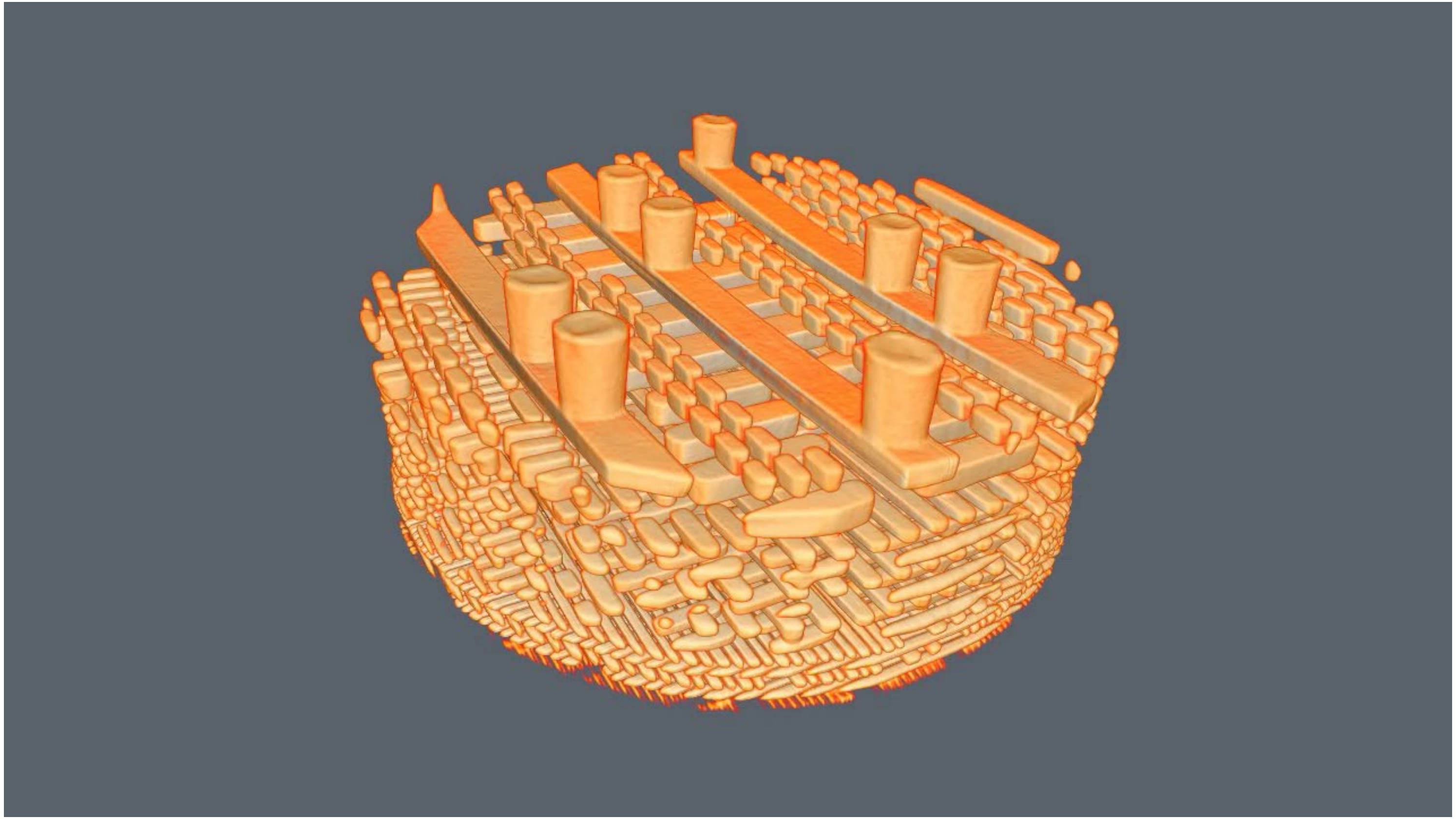

T. Aidukas, N. W. Phillips, A. Diaz, E. Poghosyan, E. Müller, A. F. J. Levi, G. Aeppli, M. Guizar-Sicairos, and M. Holler, "High-performance 4-nm-resolution X-ray tomography using burst ptychography," Nature **632**, 81 (2024)

Outline

X-ray imaging

The phase problem (CDI)

Ptychography

- Ultrafast X-ray imaging with free-electron lasers

Ultrafast X-ray imaging with free-electron lasers

Catching molecules in action

X-ray free electron lasers (X-FELs)

Diffract-before-destroy

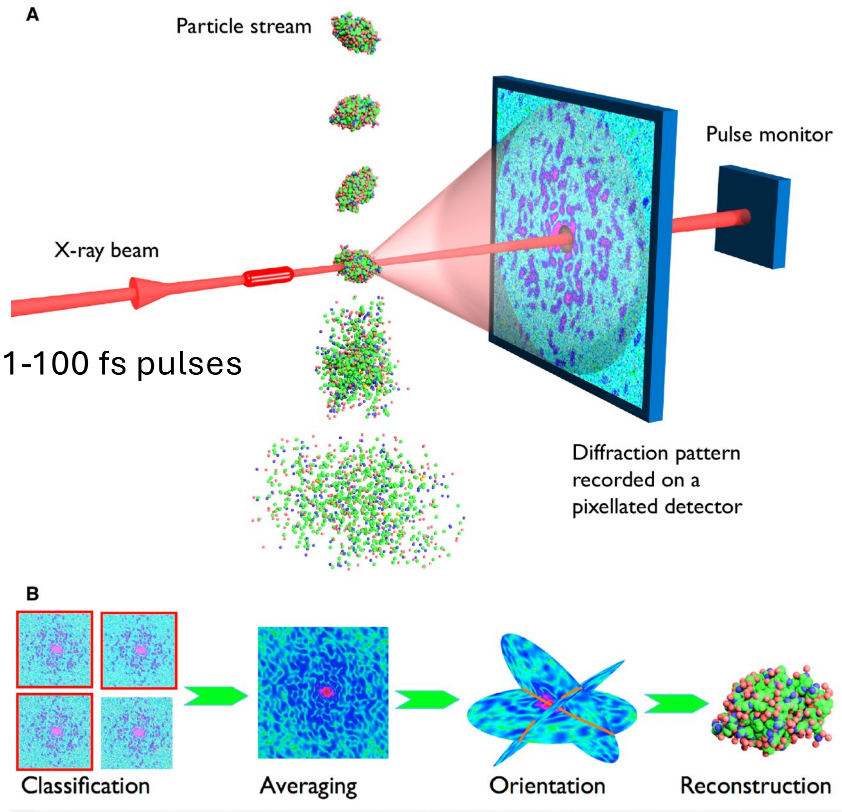

1-100 fs pulses

Image source: https://cid.cfel.de/research/single_particle_imaging/
Henry Chapman, CFEL. Science, 2007, 316, 1444-48.

Swiss FEL – Swiss Free Electron Laser @ PSI

PSI

EPFL

Innovations on the electron source enabled a compact and cost-effective design

Eduard Prat, et al. "A compact and cost-effective hard X-ray free-electron laser driven by a high-brightness and low-energy electron beam," Nature Photonics **14**, 748 (2020)

The SwissFEL movie
https://www.youtube.com/watch?v=sMWnA-vUlw0&list=PL0b-ynhMVTd4Y2wU-1B39Kpnxwg0-YmU&index=2

Ultrafast serial crystallography

Catching molecules in action

Crystals instead of single molecules

- ➢ Boost signal

Delay between laser and X-ray pulse

- ➢ Time resolution

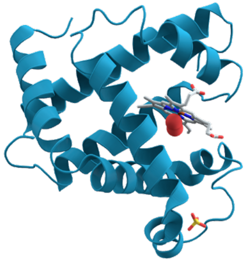

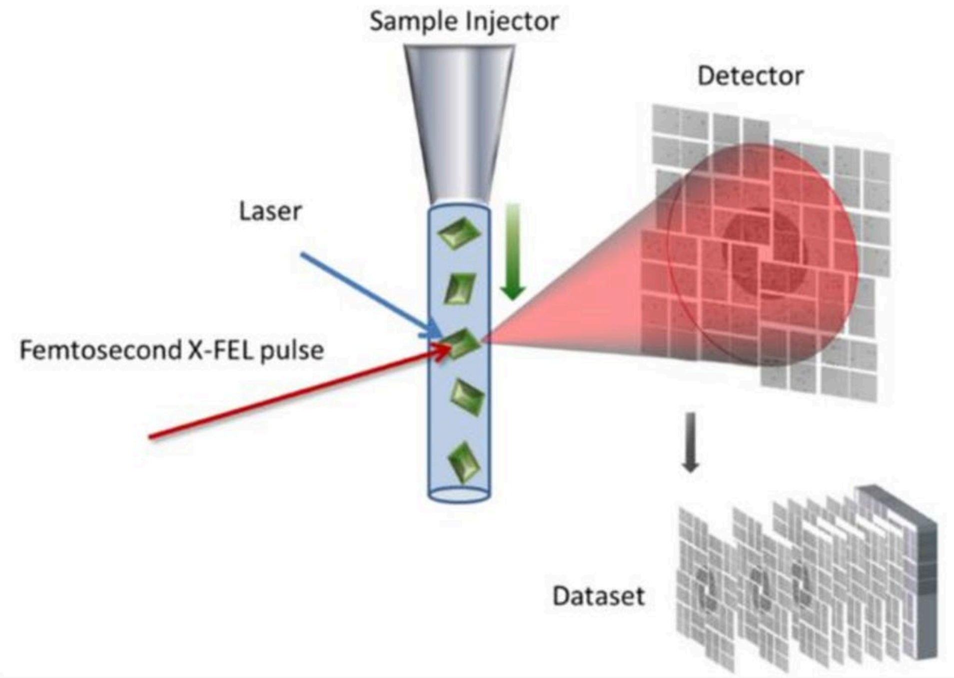

Images from: Petra Edlund, “Structural Features of Bacteriophytochromes Photoactivated Proteins Studied by Serial Femtosecond Crystallography” 2018. Myoglobin wikipedia.org

Ultrafast serial crystallography

Catching molecules in action – Light activated sodium pumps

Sodium differences (transport) plays a very important role in in the way nerve cells conduct stimuli, neurons have powerful sodium pumps in their membranes. Also important for light sensing and energy harvesting.

Static structure is known, but how do pumps change to allow the sodium ions, and only sodium ions, to be transported?

KR2 resting state

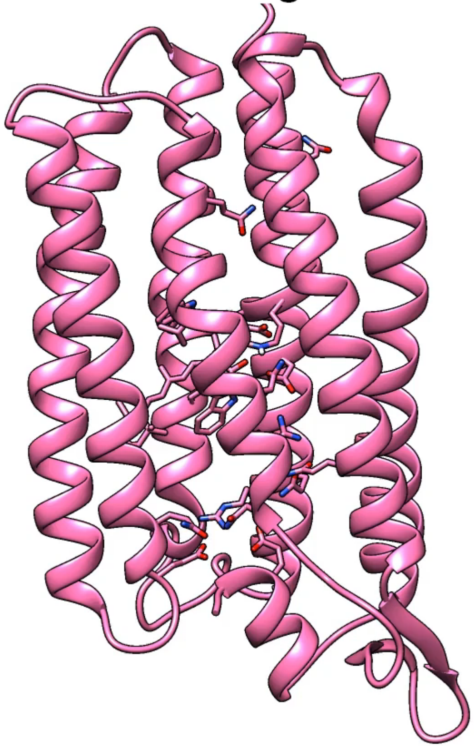

P. Skopintsev et al., "Femtosecond to millisecond structural changes in a light-driven sodium pump," Nature 583, 314 (2020)

Questions?

PSI

EPFL

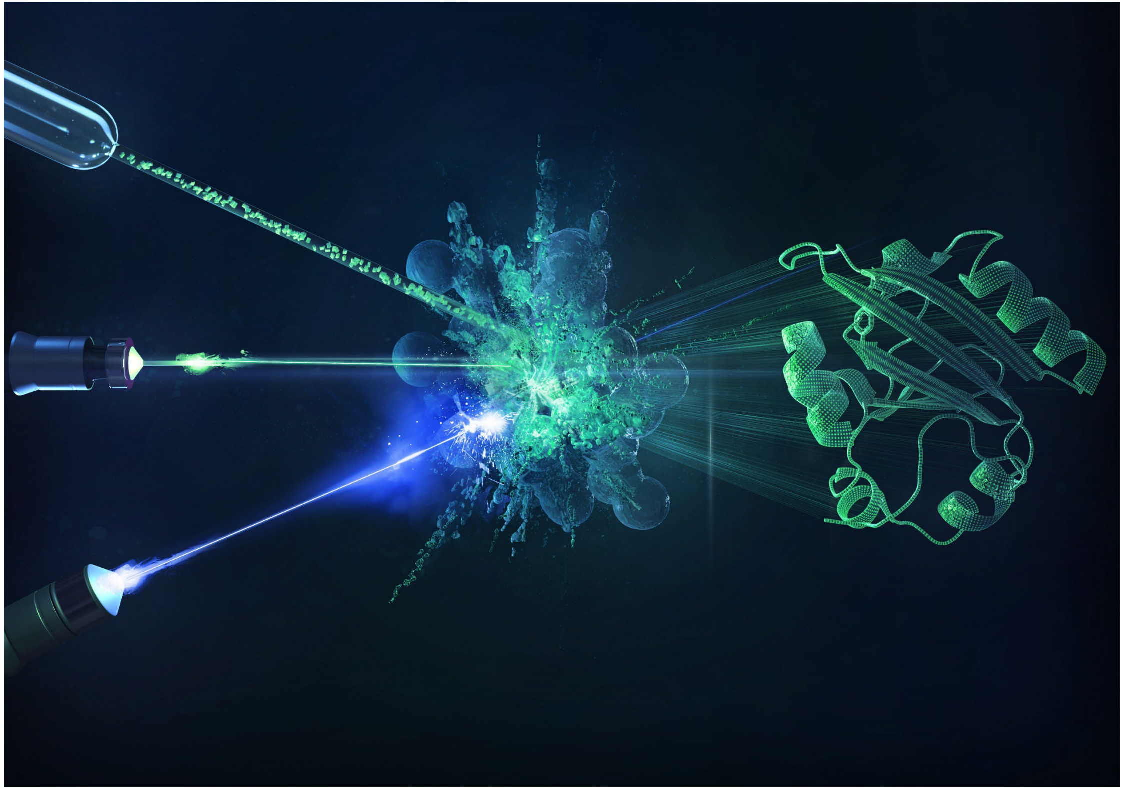

image copyright: European XFEL/Blue Clay Studios

CXI